Quaternary Science Reviews

The influence of multidecadal climate variability and abrupt landscape change on terrestrial ecosystem composition and fire regime in the Upper Columbia River Basin - a Holocene perspective

--Manuscript Draft--

Manuscript Number:	
Article Type:	Research Paper
Keywords:	Paleoclimate; paleoecology; ENSO; PDO; Pacific Northwest; fire; drought; insolation
Corresponding Author:	Samuel Mark, PhD University at Buffalo UNITED STATES
First Author:	Samuel Mark, PhD
Order of Authors:	Samuel Mark, PhD
	Cathy Whitlock
	Mark Abbott
	Byron Steinman
	Alejandro Fernandez
	Jen Steeple
Abstract:	High-resolution paleoclimatic and paleoecologic datasets from a small lake in eastern Washington help elucidate Holocene environmental dynamics in the interior Pacific Northwest. Round Lake lies near the ecotone between sagebrush steppe and dry pine forest, making it highly sensitive to changes in precipitation-evaporation (P-E) balance. We present isotopic, sedimentological, and paleoecological data from a single sedimentary sequence analyzed at sufficient resolution to detect sub-decadal climatic variability. During the early Holocene (11000-8500 BP), when summer insolation was higher than present, Round Lake experienced persistent aridity that led to reduced forest cover and small, probably frequent surface fires. Sub-centennial hydroclimate fluctuations during this period were muted, as indicated by low multi-decadal variability in δ18Ocarbonate records from the region. Oxygen isotopes indicate increased cool-season moisture during the middle Holocene (8500-5300 BP), but stratigraphic evidence suggests intermediate and variable lake levels. The deposition of the Mazama tephra (ca. 7600 BP) led to a protracted expansion of steppe at the expense of forest. Increased hydroclimate variability and fire activity following ash deposition likely restricted conifer taxa even when elevated cool-season moisture would have facilitated their growth. The late Holocene was marked by persistently high lake levels, as indicated by the lithostratigraphic and pollen records. Comparatively large multidecadal variations in precipitation, which peaked during the last millennium, were also prominent features of late-Holocene hydroclimate, and may have been related to the strengthening of the El Niño Southern Oscillation and Pacific Decadal Oscillation. Pinus and Pseudotsuga show a 60-100 year lag in their response to hydroclimatic variations inferred from the oxygen isotope records. These results highlight how millennial-to-decadal scale hydroclimate conditions, along with abrupt landscape change, influence ecology in a water-stressed region of western North America.
Suggested Reviewers:	Bryan Shuman bshuman@uwyo.edu
	John Williams jww@geography.wisc.edu

University at Buffalo The State University of New York

To the editorial board of Quaternary Science Reviews,

On behalf of my coauthors, I am excited to submit our paper "The influence of multidecadal climate variability and abrupt landscape change on terrestrial ecosystem composition and fire regime in the Upper Columbia River Basin - a Holocene perspective" for your consideration as a research article in Quaternary Science Reviews. As drought and fire in western North America put increasing strain on environmental and anthropogenic systems alike, long-term paleoclimate proxy records are increasingly valuable for their ability to shed light on climate-ecosystem interactions under different climate states. To this end, we present high-resolution records of oxygen and carbon isotopes from authigenic calcium carbonates, pollen, charcoal, mercury, organic carbon isotopes, and basic sedimentology from a lake in north-central Washington. The resolution and breadth of proxies from this sedimentary sequence represent a unique opportunity to study climate and ecological covariance over the past 11,000 years.

Oxygen isotopes from authigenic calcium carbonates have long been a valuable tool for reconstructing hydroclimate variability in the northwestern United States. We find that during the Holocene, hydroclimate varied in response to changing orbital configurations as well as Pacific ocean-atmosphere phenomena such as the Pacific Decadal Oscillation and the El Niño Southern Oscillation. Terrestrial ecology and fire activity show significant relationships to ambient climate, but tree species show lagged responses to ambient hydroclimate, sometimes of more than 100 years. The deposition of the Mazama ash layer (7600 BP) represented an abrupt, non-climatological landscape disturbance that shifted the local ecosystem into a more sagebrush-dominant mode which persisted for millennia. Our multi-proxy analysis allowed us to investigate the overlapping forces which contributed to this long-term response to a short-lived disturbance. These results have implications for the future of this already water-stressed and fire-vulnerable region.

The manuscript at present consists of 8329 words, 10 figures, 10 supplemental figures, and 105 citations. Individual author contributions are detailed below. The authors disclose no conflicts of interest. We thank you for your consideration and look forward to hearing from you. Please don't hesitate to reach out with any additional questions.

Sincerely,

Sam Mark
NSF OPP Postdoctoral Fellow
University at Buffalo, University of Alaska Fairbanks
szmark@buffalo.edu

Author contributions:

All authors contributed substantially to this manuscript. Specific contributions for each author are outlined below according to the Elsevier contributions types.

Author 1 (SZM): Conceived and designed analysis, collected data, performed analysis, wrote the paper.

Author 2 (CW): Conceived and designed analysis, collected data, performed analysis, wrote the paper.

Author 3 (MBA): Conceived and designed analysis, collected data, wrote the paper, acquired funding.

Author 4 (BAS): Conceived and designed analysis, contributed data or analysis tools, wrote the paper, acquired funding.

Author 5 (AF): Contributed data or analysis tools, wrote the paper.

Author 6: (JS): Collected data.

The influence of multidecadal climate variability and abrupt landscape change on terrestrial ecosystem composition and fire regime in the Upper Columbia River Basin - a Holocene perspective

Sam Mark, Cathy Whitlock, Mark Abbott, Byron Steinman, Alejandro Fernandez, Jennifer Steeple

Abstract

High-resolution paleoclimatic and paleoecologic datasets from a small lake in eastern Washington help elucidate Holocene environmental dynamics in the interior Pacific Northwest. Round Lake lies near the ecotone between sagebrush steppe and dry pine forest, making it highly sensitive to changes in precipitation-evaporation (P-E) balance. We present isotopic, sedimentological, and paleoecological data from a single sedimentary sequence analyzed at sufficient resolution to detect sub-decadal climatic variability. During the early Holocene (11000-8500 BP), when summer insolation was higher than present, Round Lake experienced persistent aridity that led to reduced forest cover and small, probably frequent surface fires. Sub-centennial hydroclimate fluctuations during this period were muted, as indicated by low multi-decadal variability in $\delta^{18}O_{carbonate}$ records from the region. Oxygen isotopes indicate increased cool-season moisture during the middle Holocene (8500-5300 BP), but stratigraphic evidence suggests intermediate and variable lake levels. The deposition of the Mazama tephra (ca. 7600 BP) led to a protracted expansion of steppe at the expense of forest. Increased hydroclimate variability and fire activity following ash deposition likely restricted conifer taxa even when elevated cool-season moisture would have facilitated their growth. The late Holocene was marked by persistently high lake levels, as indicated by the lithostratigraphic and pollen records. Comparatively large multidecadal variations in precipitation, which peaked during the last millennium, were also prominent features of late-Holocene hydroclimate, and may have been related to the strengthening of the El Niño Southern Oscillation and Pacific Decadal Oscillation. *Pinus* and *Pseudotsuga* show a 60-100 year lag in their response to hydroclimatic variations inferred from the oxygen isotope records. These results highlight how millennial-to-decadal scale hydroclimate conditions, along with abrupt landscape change, influence ecology in a water-stressed region of western North America.

Introduction

Water stress and wildfire activity in western North America now surpass 20th century maxima (Higuera and Abatzoglou 2021). An empirical understanding of climate-ecosystem variability during droughts of magnitudes resembling those projected for the next century must therefore rely on paleoclimate proxy data from periods that experienced conditions more extreme than those of the past 100 years. Lake sediments offer particularly useful tools for paleoenvironmental exploration, as they archive multiple physical, chemical, and biological conditions within the catchment. Oxygen isotopes from authigenic carbonate minerals (Nelson et al. 2011), pollen (Whitlock and Bartlein 1997), charcoal (Walsh et al. 2023), and lithostratigraphy (Shuman et al. 2009a) have all provided valuable insight into environmental changes in the Pacific Northwest (PNW) of North America (an area that includes WA, OR, ID, western MT, and BC), during times when orbital parameters, glacial extent, and greenhouse gas concentrations differed from those of the modern era. Typically, the greater timespan gained by using lake sediments for such research often comes at the expense of lower temporal resolution, with most studies lacking the chronological precision and sampling frequency to resolve shifts in interannual to interdecadal climate variability.

Insolation has long been implicated as a major control on millennial-scale changes in environmental conditions in North America. In the Pacific Northwest, higher-than-present summer insolation and its direct influence on temperature and evapotranspiration, as well as its indirect influence on atmospheric circulation (Bartlein et al. 1998), contributed to a warm, dry early Holocene (Lehmann et al. 2021, Chase et al. 2008). These changes were associated with major shifts in vegetation, increased fire activity, and lake level variations (e.g. Millspaugh et al. 2000, Brunelle and Whitlock 2003) and have the potential to provide valuable context for near future projections of heightened summer temperatures and aridity in the PNW (Mote and Salathe, 2010).

While long-term insolation changes drive climate and ecosystem development over millennial timescales, ocean-atmospheric phenomena such as the El Nino Southern Oscillation (ENSO) and Pacific Decadal Oscillation (PDO) impose higher-frequency (sub- to multi-decadal) variability on water balance (McAfee and Wise 2016), atmospheric circulation (Wise and Dannenberg 2017), and fire activity (Heyerdahl et al. 2008) in the PNW. Their role in Holocene hydroclimatic and ecological variability is poorly known for lack of high-resolution records. Positive ENSO (El Niño) and PDO-positive (+) phases are associated with a strengthened Aleutian Low pressure system in winter that deflects storm tracks south, causing drier-than-average conditions in the region (McAfee and Wise 2016, Barron and Anderson 2011). The opposite holds true during La Niña/PDO negative (-) phases (Fig. 1). Recent work has shown the importance of these oscillatory systems in influencing biomass burning in western North America (Mark et al. 2023, Homann et al. 2022). Periodic wet intervals are crucial for the accumulation of fine fuels (Hessl et al. 2004) and the establishment of slow-growing moisture sensitive arboreal species (Gray et al. 2006). Subsequent multidecadal periods of aridity can drive widespread fire activity (Hessl et al. 2004, Heyerdahl et al. 2008) and inhibit the encroachment of woody vegetation (Gray et al. 2006). As such, changes in the frequency and amplitude of these ocean-atmosphere phenomena may have profound implications for terrestrial ecosystem dynamics.

Here, we present a high-resolution Holocene record of climate change and ecological response from a small lake in north-central Washington (Fig. 1). Oxygen and carbon isotope measurements from authigenic calcium carbonate as well as changes in lithology, organic carbon isotopes, mercury accumulation, pollen composition, and charcoal abundance provide information about past climate variations and their influence on vegetation, fire, and landscape evolution over the last 11,000 years. Our objectives are to (1) reconstruct centennial-millennial-scale climate and ecological variations over the Holocene, primarily using a combination of $\delta^{18}O_{carbonate}$ measurements, physical stratigraphy, and pollen; (2) reconstruct changes in the amplitude and frequency of multidecadal climate phenomena as recorded in the Round Lake $\delta^{18}O_{carbonate}$ record; and finally (3) examine the role of climate variability and landscape change over multiple time scales and their role in driving ecosystem dynamics.

2.1 Study Site

Round Lake (48.61 N 119.12 W; 654 m a.s.l.; surface area ~0.07 km^2) is located in a former ice-block depression created during the recession of the Okanogan Lobe of the Cordilleran Ice Sheet (Koyanen and Slaymaker 2004). The lake bathymetry is generally flat, with a maximum depth of approximately 12 m on the eastern half of the lake. The surficial geology is calcium-rich Quaternary glacial drift, and the watershed lies within the Lime Belt of eastern Washington (Oroville Quadrangle, Fox 1970). Field surveys and satellite imagery show no significant surficial outflows. Orthophotographs taken between 1985 and 2023 also fail to show surficial outflows, including during 1998 and 2016, when nearby Castor Lake overflowed (Steinman et al. 2013, Steinman et al. 2016). The lake is perched high above the Okanogan River and is largely isolated from the regional groundwater table. The southwest-facing slope of the watershed supports *Artemisia* steppe and grassland, while the northeast-facing slope is covered by open *Pinus ponderosa* forest (Fig. 1D). At higher elevations and in wetter settings in the region, mixed-coniferous forests composed of xerophytic and mesophytic conifer taxa are dominated by *Pseudotsuga menziesii*, *Larix occidentalis*, *Pinus contorta*, and *Pinus ponderosa*, and lesser amounts of *Picea engelmanii*, *Abies grandis*, *Tsuga heterophylla*, and *Thuja plicata* (Jain et al. 2012).

The average fire-return interval in *Pinus ponderosa* forests was approximately 6 years prior to Euro-American settlement (Jain et al. 2012), but 20th century fire exclusion and cattle grazing have contributed to a decline in wildfires (Jain et al. 2012), with many dry forests experiencing century-long fire-free intervals (Walsh et al. 2018). The mixed-coniferous forests at higher elevations have historically been maintained by frequent fires (10-13 episodes 1000 years^{-1}) of different intensity and size, which has been referred to as a mixed-severity fire regime (Arno et al. 2000, Jain et al. 2012).

Round Lake receives an annual average precipitation amount of 330 mm year^{-1} (NOAA Omak weather station GHCND:USW00094197, 48.46 N 119.52 W, 397.4 m a.s.l.) of which approximately two-thirds falls during the cool season (November-March), when the Aleutian Low strengthens and moves southward, bringing cyclonic storms to the region (Rodinov 2007). During El Niño/PDO+ conditions, the Aleutian Low strengthens and the corresponding North Pacific high-pressure system inhibits storm tracks from delivering moisture to the PNW (Rodinov 2007, Bryson and Hare 1974). The opposite pattern generally occurs during La Niña/PDO- conditions.

2.2 Lithologic Analysis and Age Control

Sediment cores were retrieved in August 2017 and February 2018 from the deepest location using a modified Livingstone piston corer (Wright et al. 1984) and a freeze corer (Besonen et al. 2008, Mark et al. 2023). Piston cores were extruded into plastic tubes in the field and transported to the University of Pittsburgh Sedimentology Laboratory. Short cores were also collected in February 2018 with a freeze corer. Overlapping Livingstone cores were correlated based on lithostratigraphy, and the freeze core was compared with the Livingstone cores based on the comparison of the oxygen isotope records (see Mark et al. 2023). Water samples from Round Lake were collected near the center of the lake nine times between 2003 and 2018. Water samples were taken in plastic vials and sealed under water to ensure there was no air space. The top 100 cm of the sediment record is described in Mark et al. 2023.

Sediments were divided into lithologic units based on composition and texture according to the scheme of Schnurrenberger et al. (2003). Cores were imaged using a GeoTek line scanning camera and aligned according to the laminated visible stratigraphy. The GeoTek also provided magnetic susceptibility (MS) and color (here presented as L*, Murton and Crowhurst 2021) measurements. 1-cm^3 volumetric samples were taken at 1-cm continuous intervals and weighed, dried, and re-weighed to calculate bulk density. The remainder of the sample was then combusted at 550^{o}C for 2 hours and re-weighed to determine organic content, then re-combusted at 1000^{o}C for 2 hours; the weight loss after each respective ignition determined carbonate content and residual mineral content (Heiri, 2001).

An age model for the full sedimentary sequence was developed using a combination of ^{137}Cs, ^{14}C, and tephrochronology. The uppermost 20 cm was analyzed at 0.5 cm resolution on a Canberra BE-3825 Germanium Detector at the University of Pittsburgh. For ^{14}C dating, charcoal and seeds were selected from disaggregated sediments using a paintbrush under 3-10x magnification and subjected to an acid-base-acid pretreatment (Santos et al. 2014). Samples were subsequently combusted, graphitized and analyzed at the University of California-Irvine W.M Keck Carbon Cycle Accelerator Mass Spectrometer on a National Electrostatics Corporation

500kV 1.5SDH-1 Compact AMS device. The eruption of Mount Mazama (7537-7728 cal yr BP, Egan et al. 2015) resulted in a ~60-cm-thick ash layer. The Mazama ash was identified by its thickness and age (Steinman et al. 2019, Schiller et al. 2020, and many others). This thickness was subtracted from the overall depth of the sedimentary record to construct the final age model. Individual age control points (Table S1) were converted into an age-depth model with quantified uncertainty using the BChron program in R (Parnell et al. 2014). All ^{14}C dates were calibrated using the IntCal20 calibration curve (Reimer et al. 2020).

2.5 Isotopic Analysis

Sediment samples of 1 cm^3 were taken every half centimeter for the entirety of the core, except from the top 60 cm where they were sampled with a razor blade at a finer resolution (approximately 0.1-0.5cm) according to the visual stratigraphy of the freeze cores (see Mark et al. 2023 for a full description). Samples were disaggregated in a solution of 7% H_2O_2 to remove the labile organic fraction and then sieved through a 63-μm mesh screen to remove any remaining coarse mineral fraction and isolate $CaCO_3$. The remaining fine fraction was treated with 3% NaClO, rinsed with deionized water, lyophilized, and homogenized (Nelson et al. 2011). Prepared samples were sent to the University of Arizona Environmental Isotope Laboratory. $\delta^{18}O_{carbonate}$ and $\delta^{13}C_{carbonate}$ measurements were conducted on a Finnigan MAT 252 gas ratio mass spectrometer and are presented in standard δ-notation. 1σ precision, based on repeated measurements of NBS-18 and NBS-19 standards, are 0.1‰ for $\delta^{18}O$ and 0.08‰ for $\delta^{13}C$. Surface-water isotopes from 2016, 2017, and 2018 were measured for δ^2H_{water} and $\delta^{18}O_{water}$ at Indiana University Purdue University Indianapolis using a Picarro L2130-I Analyzer, with measurements calibrated to Los Gatos high standard ER1 and USGS low standard 49. 1σ precision was 0.6‰ for δ^2H_{water} and 0.1‰ for $\delta^{18}O_{water}$.

Total organic carbon:total nitrogen (TOC:TN) ratios and carbon isotopic analysis of organic material were measured by lyophilizing and homogenizing 1 cm^3 samples down core at approximately 4 cm resolution. Homogenized samples were then weighed and placed in silver capsules. To remove carbonate without preferentially dissolving labile organic material, samples were vaporously acidified for 6 hours (Komada et al. 2008). Samples were then combusted and analyzed on a Thermo Scientific Delta V Advantage IRMS system at the University of Pittsburgh to determine TOC:TN and $\delta^{13}C_{Organic}$. Analytical uncertainty is +- 0.5% for C concentration, +- 0.1% for N concentration, and +- 0.1‰ for $\delta^{13}C_{Organic.}$

2.6 Pollen and charcoal analysis

Samples of 1 cm^3 were taken at approximately 8-cm intervals down the length of the core for pollen analysis and were prepared using standard procedures (Bennett and Willis, 2001). Pollen residues were mounted in silicon oil and examined at magnifications of 4000 and 1000x, and at least 300 terrestrial grains were counted by level. Terrestrial pollen percentages were based on the sum of all terrestrial pollen and spores, and aquatic/riparian and nonpalynomorph percentages, including microscopic charcoal, were calculated based on a sum of all pollen and spores. A *Lycopodium* tablet of known concentration was added to each sample to calculate pollen concentration (grains cm^{-3}) and pollen accumulation rates (grains cm^{-2} yr^{-1}).

Pinus pollen grains with an intact/preserved distal membrane were identified as either *Pinus* subgen. *Pinus,* attributed to *P. Ponderosa* and/or *P. contorta*, or *Pinus subgen. Strobus*, ascribed to *P. monticola*, which grows in the region, or *P. albicaulis* found at higher elevations. *Abies* grains were assigned to *A. grandis* or the higher elevation *A. lasiocarpa*. The source of Cupressaceae pollen was *Juniperus communis*, *J. scopulorum*, and/or *Thuja plicata*. *Pseudotsuga*-type pollen was assigned to *Pseudotsuga menziesii*, which grows in the watershed, although *Larix occidentalis* and *L. lyallii* are also present at higher elevations in the region. Cyperaceae was considered an aquatic/riparian taxa at this site.

Samples of 1 or 2 cm^3 were collected every 4cm for charcoal analysis and prepared according to the methodology of Whitlock and Larsen (2001). Samples were disaggregated for

24 hours in a mix of sodium hexametaphosphate and bleach and sieved through a 125-µm mesh screen. Charcoal fragments above this size were counted on a light microscope under 4-10x magnification and converted into charcoal accumulation rates (CHAR, pc cm^2yr^{-1}). The sampling frequency was sufficient to document general fire trends, not individual fire events that occurred interannually prior to Euro-American settlement in the region (Jain et al. 2012).

In addition to the new pollen data from Round Lake, *Pinus, Picea, Pseudotsuga, Artemisia,* Poaceae*,* and Cyperaceae pollen percentages published by Mack et al. (1976, 1978a, b, c, 1979, 1983) were digitized, and ^{14}C chronologies were recalibrated. New age-depth models were generated in the same manner previously described for Round Lake.

2.7 Mercury analysis

Mercury (Hg) levels in lake sediments are ultimately derived from multiple anthropogenic and environmental processes (Pompeani et al. 2018). Here, Hg was analyzed to shed light on both biomass burning, which volatilizes mercury bound in soil and vegetation, and is transported to the lake largely through atmospheric deposition (Biswas et al. 2007), and small-scale gold mining, which generally relies on mercury to extract gold from ore (Esdaile and Chalker 2018). Hg samples were taken at approximately 8 cm resolution and lyophilized, homogenized, and assayed on a DMA-80 Direct Mercury Analysis System. Hg concentrations (ug/kg) were converted to accumulation rates (ug/cm^2yr^1) by dividing concentration by the age range spanned by each individual sample and subsequently by the bulk density of that sample.

2.8 Statistical analysis

Canonical correspondence analysis (CCA) was conducted in R using the package 'vegan' (Oksanen et al. 2013). $\delta^{13}C_{Organic,}$ $\delta^{13}C_{CaCO3}$, and % organic explained the highest degree of inertia (analogous but not identical to variance; see Wagner 2004) in the pollen dataset and were used for the CCA. Because all samples came from the same cores, correlations were performed on real (non-interpolated) increments, eliminating relative age uncertainty. For comparison of antecedent climate conditions to pollen spectra, oxygen isotope samples were interpolated to constant 10-year increments to achieve consistency in the time domain (Fig. 10). This interval was selected because the $\delta^{18}O_{carbonate}$ sampling rate is finer than 10 years throughout the entire sequence. The pollen data were not interpolated to minimize the introduction of unwanted artifacts into the correlations. Where appropriate, effective degrees of freedom were estimated when calculating correlations between time series according to the formula (1+p)/(1-p) where p is the lag-1 autocorrelation (Bretherton et al. 1999). Moving variances for $\delta^{18}O_{carbonate}$ records were calculated by interpolating samples to constant 8-year time steps (justified given the median temporal resolution of each proxy record) and calculating the variance in 9-sample (72-year) sliding windows. This interval is suitable for capturing patterns of multi-decadal variability described by Newman et al. (2016). Varying window sizes between 56-96 years did not substantially alter results. Wavelet analysis was carried out on the same linearly interpolated dataset using the MATLAB code developed by Torrence and Compo (1998). Cross-wavelet analysis was carried out in MATLAB using the code developed by Grinsted et al. (2004). For both wavelet and cross-wavelet, significance intervals were estimated using 1000 random autoregressive models comparable to the observed dataset (Grinsted et al. 2004). The Climate Data Toolbox for MATLAB (Greene et al. 2019) and scientific colormaps from Crameri (2018) were used for plotting.

Results

3.1 Chronology

The ^{137}Cs and ^{14}C constrained age model suggest the sedimentary sequence spans the years -68-10950yr BP. The overall sedimentation rate averaged approximately 0.07 cm/yr. From the bottom of the core to 730 cm depth (8410 yr BP 2σ+-130 yr) the sedimentation rate averaged approximately ~0.03 cm/yr. Between 730 cm and 314 cm depth (4950 yr BP 2σ+-140 yr) the sedimentation rate reached maximum Holocene values of 0.4 cm/yr. Above 314 cm, sedimentation rates returned to values of approximately 0.03 per year.

3.2 Lithology

Three distinct lithologic units in the Round Lake sequence were delineated based on visual inspection and abrupt changes in mass accumulation rate of $CaCO_3$ (Fig. 2). The bottom unit (Unit I, 800-730 cm depth, 2σ 10760-11140 to 2σ 8280-8540 BP) of the stratigraphic sequence consists of dense, banded packages of alternating dark organic-rich peaty sediment and light-colored carbonate-rich silty- to sandy- clay (Fig. 2). The middle unit (Unit II, 740-314 cm depth, 2σ 8283-8543 BP to 2σ 4809-5091 BP) is composed of light-colored banded and mottled calcareous (>30% $CaCO_3$) sediments. Unit II is interrupted by an approximately 60 cm-thick Mazama ash deposit between 606-666 cm depth. Carbonate-rich sediments predominate immediately above the Mazama ash, with thick (10-20 cm-scale) calcareous bands interspersed with finer (mm-scale) laminations (Fig. S1). The uppermost Unit III (314-0 cm depth; 2σ 4809-5091 BP), begins with a sharp transition from calcareous-rich banded sediments to dark colored finely laminated sapropel. This unit is rich in $CaCO_3$, but less so than Unit II, (12%-65%). The sedimentation rate (0.4 cm/yr) was highest in Unit II (Fig. 2). Both carbonate and organic mass accumulation rates were highest in Unit II; however, the percentage of organic matter is low compared to carbonate due to the high carbonate production rates (Fig. 2). This suggests that the high sedimentation rate was primarily driven by enhanced deposition and preservation of authigenic carbonates.

3.3 Carbon and Oxygen Isotopes

Water taken from Round Lake between 2006-2018 had $\delta^{18}O_{water}$ values that ranged between -6.9 and -11.2 ‰ and was evaporatively enriched with respect to local meteoric water (annual average of -12.9‰) and ground water (-15.8‰) by several per mil (Fig. S3). Round Lake therefore loses significant water to evaporation (Fig S3. Mark et al. 2023). This is further supported by the lack of a visible surficial outflow during field surveys or satellite imagery.

$\delta^{18}O_{carbonate}$ values range between -14.0‰ and -8.3‰ over the course of the record. Unit I has the most enriched $\delta^{18}O_{carbonate}$ values, averaging -10.7‰. Unit II has the lowest overall mean $\delta^{18}O_{carbonate}$ of -11.4 ‰. More depleted $\delta^{18}O_{carbonate}$ values in this unit corresponds with darker, more organic-rich sediments (Fig. S2). Unit III has a mean $\delta^{18}O_{carbonate}$ value of -11.3 ‰ (Fig. 3A). $\delta^{13}C_{carbonate}$ values vary between -0.8‰ and -6.8‰ and are significantly positively correlated with $\delta^{18}O_{carbonate}$ ($r=0.53$, $p=<0.01$) throughout the entire record (Fig. 3B), typical of most evaporatively enriched water bodies (Li and Ku 1996).

3.3 Organic Matter Isotope Measurements and TOC:TN

TOC:TN ratios vary between 10-14 for the duration of the record, and generally increase up core (Fig. S4). In Unit I, $\delta^{13}C_{Organic}$ values are approximately -31‰ (Fig. S4). $\delta^{13}C_{Organic}$ values reach their maximum level of -27‰ in Unit II at 365 cm depth (Fig. S4). After the peak at 6000 BP, $\delta^{13}C_{Organic}$ declines in Unit III, to minimum values (-33‰) at 265 cm depth. Values are increasingly variable and generally more enriched above 200 cm depth (Fig. S4).

3.4 Pollen and Charcoal

The pollen record was divided into two major pollen zones based on the results of a constrained cluster analysis (CONISS, Grimm 1987). Zone RL-1 (769-446 cm depth; 11,060-6400 cal yr BP) are characterized by high percentages of *Artemisia* (15-27%), with exceptionally high values (34-51%) just above the Mazama ash (621-597 cm). *Pinus* values are moderate (20-48%), with the identifiable grains almost exclusively from *P*. subgen. *Pinaceae* (e.g. *P*. *ponderosa* or *P*. contorta). Poaceae values are also relatively high (4-21%) in this zone; *Alnus rubra*-type reach moderate values (4-9%); and *Abies*, *Pseudotsuga*-type, *Alnus viridis* subsp sinuata-type, *Betula*, and *Salix* pollen are present in low values (each <3%). Among the other nonarboreal taxa, percentages of Asteraceae Asteroideae undiff. (<5%) and Amaranthaceae (<2%) are low with little variability. Cyperaceae pollen was well represented (3-11%) among the aquatic/wetland taxa. Microscopic charcoal percentages are moderate in this zone, and the highest values occurred at 718 cm depth (9450 BP) and between 517 and 480 cm depth (immediately above the Mazama ash).

Zone RL-2 (446-8.5cm depth; 6410 - -10 BP) features an increase in *Pinus*, *Abies*, and *Pseudotsuga*-type, and a decline in *Artemisia* percentages. The identifiable *Pinus* grains are *P*. subgen. *Pinaceae*. *Alnus* rubra-type values are lower at the base of the zone and reach highest values (up to 12%) towards the top. Poaceae and *Asteraceae Asteroideae* undiff. percentages are low, reaching <1% before 4000 cal yr BP and then rise to 11-20% in the last 1000 years. This recent increase in herbaceous taxa is associated with a prominent rise in aquatic *Myriophyllum* pollen (up to 34%) after 4000 cal yr BP and a concomitant decline in Cyperaceae (<10%). Microscopic charcoal percentages were steady but low in this zone.

CHAR (>125 μm fraction) vary between 0-60 pc/cm^{2}yr over the entire record, while microscopic charcoal percentages vary between 0-24 %. Both size fractions were relatively low between 800-676 cm depth (Units I and II, Zone RL-1), although the >125 μm fraction reach a local maximum between 760-736 cm depth (9190-8510 BP), and micro-CHAR reach a local maximum between 760-700 cm depth (9190-7920 BP).

Both datasets reach maximum values during Unit II, with an abrupt transition to higher values immediately after the deposition of the Mazama ash. CHAR is particularly high between 676-485cm (7580-6720 BP) and 429-317 cm depth (6300-5500 BP). CHAR and micro-CHAR return to generally lower values during Unit III. Between 70 cm depth and the sediment-water interface (435 BP-present), CHAR values are generally high (see Mark et al. 2023 for further description of Round Lake CHAR during the past millennium). The correlation between CHAR and micro-CHAR is 0.55 over the entirety of the record (p<0.01).

<u>3.5 Mercury accumulation</u>

Mercury accumulation rates are lowest in Unit I and are low in Unit II below the Mazama ash. Values increase to their pre-modern maxima at approximately 6000 BP and decline abruptly thereafter (Fig. 9, Fig. S5). Values increase very sharply at (100 BP, CE 1850) to approximately 50 times the Holocene average and are elevated through the 20th century (Fig. S5).

Discussion

Changes in Round Lake lithology, oxygen isotope data, pollen percentages, and charcoal accumulation rates yield insights about the coevolution of climate and ecosystem dynamics in north-central Washington over the Holocene. First, we discuss millennial-scale changes in climatic and ecological conditions based on lithological, oxygen isotopes, and pollen data (Section 4.1). We next examine high-frequency changes in the Round Lake $\delta^{18}O_{carbonate}$ record in the context of broad-scale Pacific ocean-atmospheric phenomena (Section 4.2). Lastly, we evaluate changes in regional vegetation and fire activity (derived from pollen spectra and charcoal accumulation rates) in the context of millennial- to decadal-scale climate change and short-term landscape disturbance (Section 4.3).

4.1 Holocene-scale trends in hydroclimate

4.1.1 Early Holocene (11000-8200 BP)

Both physical stratigraphy and $\delta^{18}O_{carbonate}$ suggest persistent drought during the early Holocene. Sedimentary facies of closed-basin lakes reflect changes in lake level driven by shifting P-E balance (Schnurrenberger et al. 2003). Coarser sediments typically indicate relatively shallower depositional environments, as increased energy is required to carry larger particles towards the center of the lake (Shuman et al. 2009a). Finely laminated sapropels, conversely, indicate the lower energy depositional settings of deeper waters, where wave energy is insufficient to disturb fine layering. The stratigraphy throughout Unit I is dense and peat-like, with abundant root material in darker organic horizons. The pollen record from Round Lake suggests steppe vegetation throughout the period of Unit I, based on elevated percentages of *Artemisia* and Poaceae and low values of mesophytic conifer taxa (Fig. 5).

Oxygen isotopes in this unit are enriched compared to the rest of the record. Hydrological modelling results by Steinman and Abbott (2013) indicate that the amount of cool-season precipitation is the dominant driver of $\delta^{18}O_{water}$ and $\delta^{18}O_{carbonate}$ content of small closed-basin lakes in the PNW. A $\delta^{18}O_{carbonate}$-derived drought index from nearby Castor and Lime lakes, which accounts for changes in the isotopic composition of incoming precipitation, also shows prolonged drought throughout the early Holocene (Lehmann et al. 2021, Fig. 6). Both lake records are consistent with paleoclimate model simulations that suggest winter storm tracks were deflected away from the PNW during the early Holocene (Bartlein et al. 2014). Elevated summer insolation also promoted warmer-than-present summers with greater evaporation, consistent with chironomid and diatom-based evidence of lower lake levels from Southern British Columbia (Mushet et al. 2022, Chase et al. 2008, Fig. 6) and pollen evidence indicative of ecosystems adapted to warm, dry conditions (Brown and Hebda 2002, Hebda 1995). Data from Round Lake therefore supports other records that show reduced precipitation during cool-seasons and increased evaporation during warm-seasons, drastically decreasing annual P-E balance in the early Holocene.

4.1.2 Middle Holocene (8200-5300 BP)

The light brown, coarsely bedded carbonate muds that are interspersed with light-yellow, fine (<0.1 cm) laminae, found throughout Unit II imply intermediate and fluctuating lake levels in the middle Holocene. The $CaCO_3$ accumulation rate is very high throughout in Unit II (Fig. 2). High winter precipitation during the middle Holocene, inferred from the $\delta^{18}O_{carbonate}$ record (Fig. 6) and supported by other sites in the region (Lehmann et al. 2021) may have also increased runoff and provided abundant Ca^{2+} ions for carbonate precipitation, which is likely the limiting element in $CaCO_3$ production, as determined from other carbonate producing lakes (Nelson et al. 2011, Shapley et al. 2005). While the $\delta^{18}O_{carbonate}$ data suggest high cool season precipitation, lake level indicators suggest intermediate positions, possibly owing to enhanced warm-season insolation (Fig. 6). Many studies have found enhanced production and preservation of carbonates in intermediate lake-level settings (Anderson et al. 2005, Dean 1999). Although $\delta^{13}C_{Organic}$ values in Unit II remain in the range of C3 vegetation (-33.2‰ to -

26.6‰), the most isotopically enriched organic carbon values of the Holocene occur at approximately 6000 BP (Fig. S4), when the lithology indicates low-to-intermediate lake levels. Increased primary productivity and more complete biological sequestration of isotopically light carbon may explain the increase in organic C isotope values and suggest hot summers with intermediate lake levels (Hillman et al. 2018, Hodell and Schelske 1998). Enriched $\delta^{13}C_{Organic}$ values may also partially reflect a greater contribution from C4 and aquatic sources (Fig. S4, Meyers and Lallier-Verges, 2002). Pollen percentages show a modest increase in Cyperaceae during the middle Holocene, and a dramatic increase in *Artemisia* after the Mazama tephra (see section 4.3.4), that is sustained through the upper part of Unit II (Fig. 5). Summer insolation during the middle Holocene was higher than present at 50° N, which caused warmer, more evaporative conditions during the summer months (Fig. 6). Paleoclimate model simulations indicate a strengthened eastern Pacific subtropical high (Diffenbaugh et al. 2006), which would have further suppressed warm-season precipitation. Supporting these inferences, a chironomid-based July temperature reconstruction from Windy Lake, BC, and diatom-derived lake level reconstruction from Roche Lake, BC indicate warm summers and relatively low lake levels into the middle Holocene (Fig. 6). Conversely, a diatom reconstruction from Felker Lake, BC, records the highest lake levels of the Holocene between 7000-6000 BP (Galloway et al. 2011. Fig. 6).

The middle Holocene was likely marked by enhanced winter precipitation combined with warmer, drier summers than present. $\delta^{18}O_{carbonate}$ is lowest during Unit II, indicating increased cool-season precipitation. Steinman et al. (2016) suggest that the PNW experienced greater hydroclimatic seasonality between 7500-2500 BP, consistent with these results. Studies of Crevice Lake, WY and Castor Lake, WA, also pair $\delta^{18}O_{carbonate}$ measurements with pollen data (Crevice Lake, Whitlock et al. 2012) and lithologic data (Castor Lake, Lehmann et al. 2021, Steinman et al. 2019, Nelson et al. 2011). Sedimentary facies from Castor Lake indicate low stands until 6200 BP. Oxygen isotope minima from Castor Lake occur shortly after this, between

5800-5000 BP, overlapping with intermediate lake levels and depleted $^{18}O_{carbonate}$ at Round Lake (Lehmann et al. 2021). $\delta^{18}O_{carbonate}$ from Crevice Lake, WY also indicates wetter winter conditions between 7500-2500 BP than 2500-0 BP (Whitlock et al. 2012). Pollen assemblages from Crevice Lake, however, suggest more open vegetation and drier-than-present conditions during this period, supporting an interpretation of heightened seasonality across the region. Increased winter precipitation during the middle Holocene may have resulted from multi-millennial scale changes in the tropical Pacific Ocean-atmosphere system, with mean state conditions broadly La Niña/PDO negative-like between 8000-4200 BP (Barron and Anderson, 2011). A reduced east-west temperature gradient in the tropical Pacific (Koutavas and Joanides, 2012) and persistently cooler northeast Pacific SSTs (Praetorious et al. 2020) during a largely La Niña/PDO negative-like middle Holocene would have produced generally wetter cool-season conditions (Fig. 6). In summary, millennial-scale shifts in Pacific Ocean-atmosphere conditions likely increased the amount of incoming cool-season precipitation throughout the PNW, while elevated summer insolation and the attendant strengthening of the northeast Pacific sub-tropical high increased evapotranspiration and blocked incoming moisture during warm, arid summers. These factors led to enhanced seasonality of precipitation and larger seasonal to interannual lake-level variability.

<u>4.1.3 Late Holocene (5300 BP-present)</u>

The finely laminated, alternating black organic- and carbonate-rich sapropels interspersed with light yellow, carbonate-rich layers in Unit III indicate high lake levels in the late Holocene (Fig. 2, Fig. S1). The preservation of fine (mm-scale) laminae for the entirety of this unit suggests persistently high lake levels during the late Holocene. Despite this, $\delta^{18}O_{carbonate}$ values indicate a slight drying trend over the past 6000 years, with much more variable conditions over the last millennium, consistent with data from nearby Castor Lake (Nelson et al. 2011, Lehmann et al. 2021 Fig. 6). A decrease in the seasonality of precipitation (i.e. proportionally greater precipitation during the late Holocene compared to the middle Holocene) could also explain generally increasing $\delta^{18}O_{carbonate}$ values. A trend toward cooler, less evaporative summers is consistent with nearby temperature and lake level reconstructions (Chase et al. 2008, Mushet et al. 2022, Fig. 6), and is also consistent with modeled responses to changing orbital configuration (Bartlein et al. 2014).

The Medieval Climate Anomaly (MCA: 1000-700 BP) at Round Lake featured lower $\delta^{18}O_{carbonate}$ values than the subsequent Little Ice Age (LIA 500-100 BP) (Mark et al. 2023). This pattern is similar to $\delta^{18}O_{carbonate}$ records from several other sites in the PNW (Steinman et al. 2014, Steinman et al. 2012), which suggests that while summer temperatures may have been high during the MCA, cool-season precipitation in northwestern North America was also elevated. This pattern contrasts with tree-ring based reconstructions from southwestern North America which indicate the period was marked by widespread and persistent megadroughts (Meko et al. 2007, Cook et al. 2004). While charcoal accumulation at Round Lake is higher during the LIA compared to the MCA, consistent with several other sites from the area (Mark et al. 2023, Walsh et al. 2023, Walsh et al. 2018), pollen percentages do not indicate significant shifts in the composition of the forest over this period (Walsh et al. 2018, Fig. 5).

4.2 High-resolution climate variability in northwestern North America

The degree to which mid-latitude multidecadal hydroclimatic phenomena are internal to the climate system or are driven by external forcing mechanisms, such as periodic volcanic eruptions and anthropogenic aerosol emissions remains unclear (Mann et al. 2021, Sun et al. 2022). Oxygen isotope measurements, made at sufficiently high temporal resolution, can detect not just changes in the climatic mean state, but also changes in the amplitude or frequency of multidecadal variability. Nearby Castor Lake, WA also contains a well-studied high-resolution $\delta^{18}O_{carbonate}$ record spanning the Holocene that shows long-term changes PDO-scale phenomena (Lehmann et al. 2021, Steinman et al. 2019, Nelson et al. 2011). During the early Holocene, multidecadal variability was low in both the Round and Castor Lake $\delta^{18}O_{carbonate}$ records, and both records are entirely devoid of significant multidecadal periodicities (Fig. 7, Fig.

S8). The low variability of the $\delta^{18}O_{carbonate}$ data are unrelated to sedimentation rate, sampling interval, or lithology and are therefore interpreted as reflecting a true climatic signal. Significant multidecadal variability at Castor and Round lakes only appears at approximately 7000 BP. Both sites exhibit some significant PDO-scale (defined more strictly as 20-30 years) oscillations between 7000-5000 BP (Fig. 7C). Marine sediment cores suggest persistently La Niña/PDO negative-like conditions throughout the Pacific during the middle Holocene (Barron and Anderson 2011, Koutavas and Joanides 2012), which would have increased cool-season precipitation at Castor and Round Lake. While depleted $\delta^{18}O_{carbonate}$ values between 7000-5000 BP support the notion of generally wetter conditions, the region also apparently experienced PDO-scale oscillations between relatively wet and dry conditions.

Why there was low multidecadal variability prior to 7000 BP is not clear; a major reconfiguration of atmospheric circulation patterns in the North Pacific at approximately 8000 BP may have weakened the Aleutian Low and shifted it to a more westerly position (Lasher et al. 2021). Metcalfe et al. (2015) also document a transition occurring at approximately 8000 BP associated with the decay of lingering ice sheets, which allowed the Pacific westerlies to penetrate further north. Increased sensitivity to the strength and location of Pacific storm tracks after this time may be responsible for enhanced multidecadal variability evident in the Castor and Round Lake $\delta^{18}O$ records; the timing of these respective changes, however, is approximately 1000 years apart. Laminated sediments from the Santa Barbara Basin documenting El Niño-driven runoff show low interannual hydroclimate variability prior to 4400 BP, and a stepwise increase after this time in response to a stronger Aleutian Low enhancing the teleconnection between the tropics and mid-latitude North America (Du et al. 2021). This shift occurs more than two millennia after the transition to greater variability seen in Castor and Round lakes.

The amplitude of ENSO-driven sea-surface temperatures influences PDO-scale climate phenomena in the northern mid-latitude Pacific via the atmospheric bridge (Alexander et al.

2002). To test the long-term relationship between ENSO strength and multidecadal climate variability, we compare the $\delta^{18}O_{carbonate}$ cross-wavelet from Castor and Round lakes (which shows periods marked by significant multidecadal oscillations) to the Palmyra Atoll coral record of ENSO variability (Grothe et al. 2020, Cobb et al. 2013). When ENSO variance recorded by the corals was high, Castor and Round lakes shared significant periodicities in the 16-32 year band (Fig. 9). Between 5000-3000 BP, coral and sclerosponge records, including those from Palmyra Atoll, show a large decrease in ENSO variance (Emile-Geay et al. 2016). Decadal oscillations in the Castor and Round Lake $\delta^{18}O$ records were largely absent then, with the only significant periodicities being 64-years or longer (Fig. 9). When ENSO variance was high, interdecadal oscillations in the PDO periodicity range appear to have been a significant feature of mid-latitude hydroclimate. These comparisons demonstrate how ENSO variability, originating from the tropical Pacific, influenced multidecadal variability in the PNW.

4.3 Ecosystem responses to Holocene climate change

4.3.1 Ecosystem response to millennial-scale climate change

Pollen spectra from Round Lake, as well as other sites in the interior northern Rocky Mountains, are consistent with arid warm conditions in the early Holocene. Elevated *Artemisia,* Poaceae, and other herbaceous pollen percentages at Round Lake (Fig. 5), indicating expanded sagebrush steppe, are a consistent feature of most pollen records from eastern Washington, northern Idaho, and western Montana (Fig. S6, Mack et al. 1976, Mack et al. 1978a, Mack et al. 1978b, Mack et al. 1978c, Mack et al. 1979, Mack et al. 1983 Alt et al., 2018, Brown and Hebda 2002, Hebda 1995). Low levels of charcoal and Hg accumulation suggest reduced fire activity, or probably more low-severity surface fires between 11,000-7000 BP (Fig. 4, Fig. S7). Surface fires in steppe and grassland settings produce less charcoal than high-severity crown fires in forests (Mustaphi and Pisaric 2014). Low charcoal values during the early Holocene may therefore reflect relatively frequent, but low severity burning that was largely limited by fuel availability.

Pinus pollen percentages decline to minimum values immediately after the Mazama ashfall (see section 4.3.4) and increase to maximum values at approximately 5000 BP. *Pinus, Picea* and *Pseudotsuga* expansion occurred throughout the inland PNW during the middle Holocene, probably in response to greater precipitation and reduced evaporation relative to the early Holocene (Fig. S6). Charcoal abundance and Hg concentrations were also higher in the middle Holocene than the early Holocene, with periods of high fire activity between 7500-6700 BP and again between 6300-5500 BP. These charcoal maxima suggest more stand-replacing fires, a finding that is consistent with pollen evidence of increased mesophytic conifer taxa.

In the late Holocene, closed pine-dominated forest with some mesophytic conifers (e.g., *Picea*, *Abies*, *Pseudotsuga*) developed near Round Lake (Fig. 5, Fig. S8). This shift is consistent with the onset of cooler, wetter conditions during spring and summer, allowing for the encroachment of woody vegetation. Increased percentages of *Myriophyllum*, an aquatic species, and the decline of Cyperaceae values suggest a shift to higher lake levels after 5000 BP and particularly after 1000 BP, somewhat inconsistent with increasing $\delta^{18}O_{carbonate}$ (Fig. 5). Charcoal accumulation rates are generally lower than during the middle Holocene (Fig. 4), indicating reduced fire activity during the transition to greater forest cover and higher lake levels. Fire activity was lower during the MCA than during the subsequent LIA, a pattern noted in other CHAR records from the interior PNW (Mark et al. 2023, Walsh et al. 2023, Walsh et al. 2018, Long et al. 2019). Hg accumulation mirrors trends in charcoal abundance for much off the late Holocene but increases substantially at approximately 1850 CE. This rise coincides with the onset of gold mining in the Cascade Range to the west (Helmer et al. 2020). Small-scale gold mining is the largest global source of anthropogenic Hg emissions, as these techniques generally involve adding elemental Hg to sediments to isolate gold, which is then transported atmospherically (Eagles-Smith et al. 2018). The post 1850 increase in Hg at Round Lake is more than six times the previous Holocene maximum (Fig. S5). Anthropogenic activity, not wildfires, has likely been the dominant source of Hg after 1850 CE.

4.3.2: Climate-vegetation relationships on long and short timescales

Pollen percentages are significantly correlated to several isotopic and sedimentological proxies (Fig. 8). Lower $\delta^{18}O_{carbonate}$ values, interpreted as reflecting increased cool-season precipitation (Steinman and Abbott, Steinman et al. 2016), are associated with higher percentages of arboreal pollen. These values, however, do not meet the threshold for statistical significance ($p<0.1$). *Artemisia* and Poaceae pollen, conversely, exhibit a significant positive correlation with $\delta^{18}O$.

Pollen correlations are almost uniformly stronger when compared to $\delta^{13}C_{carbonate}$ (Fig. 8). Most studies of oxygen and carbon isotopes in lacustrine carbonates focus on oxygen isotopes (Horton et al. 2016). In closed or semi-closed systems like Round Lake, evaporation acts to enrich oxygen isotope content. Primary productivity and input of $\delta^{13}C$-depleted terrestrial sources are the major controls on $\delta^{13}C_{carbonate}$ values. The dissolved inorganic carbon pool, small compared to the oxygen pool, may be disproportionately influenced by high rates of primary productivity during long, warm summers. These same summer conditions may be particularly crucial in inhibiting the encroachment of woody vegetation. The high correlation between pollen and $\delta^{13}C_{carbonate}$ compared to $\delta^{18}O_{carbonate}$ may then owe to greater shared growing season controls on the dissolved inorganic C pool and the vegetation.

4.3.3 Ecosystem response to multidecadal climate variability

In regions that experience pronounced climate variability, terrestrial ecosystems do not exist in equilibrium with ambient climate conditions (Williams et al. 2022, Svenning and Sandel 2013). To test for lags in vegetation response to climate change, we correlated pollen values to the means of $\delta^{18}O_{carbonate}$ values of preceding samples (see Fig. S10 for schematic illustration of methodology). $\delta^{18}O_{carbonate}$ averages with window lengths of 90-140 years prior to a particular pollen sample produce the highest correlations for arboreal pollen (*Pinus, Pseudotsuga-type,* and *Picea)* and CHAR data, (Fig. 10a). Arboreal taxa and CHAR show a trend towards higher correlations with increasing window lengths (Fig. 10a) up this 90-140 year maxima. This suggests that forest taxa in the study area have consistently lagged climate change on multi-decadal time scales and are never fully in equilibrium with climate.

Williams et al. (2002) used cross-correlation analysis to demonstrate similar (approximately 100-year) lag-times between arboreal pollen and $\delta^{18}O_{chironomid}$ during the glacial-interglacial transition at 11 sites in northern Europe and eastern Canada. The Round Lake data demonstrate that temporal lags in ecological-climate equilibria (1) are a persistent feature of conifer forest history, and not just a response to a particular climate event; and (2) can result from changes in moisture balance, as indicated by $\delta^{18}O_{carbonate}$ in addition to temperature alone (see Shuman et al. 2009b).

In contrast, *Artemisia* and Poaceae are seemingly less sensitive to antecedent P-E balance than the arboreal taxa (Fig. 10). The difference between the equilibrium r-value and maximum r-value are lower for the herbaceous pollen and lack the increasing correlation structure seen in the arboreal taxa (Fig. 10). This is consistent with modern modelling (Verbruggen et al. 2021) and experimental results (Winkler et al. 2019, Gherardi and Sala 2015) that indicate nonarboreal taxa respond to hydroclimate change on sub-decadal timescales.

Multidecadal climate variability has previously been shown to influence fire activity in the western United States (Mark et al. 2023, Cooper et al. 2021, Homann et al. 2022). Wet periods are conducive to the production and connection of fine fuels, which subsequently burn during multidecadal droughts. Fire activity during the warm, dry early Holocene was likely fuel limited with an apparent absence of the periodic moist episodes which characterize the region today (Fig. S6). Low-severity, surface fires would have dominated semi-arid landscapes in the absence of wet periods to promote woody fuel accumulation. Charcoal abundance and Hg accumulation both increas with the onset of multidecadal climate variability at approximately 7000 BP and decline again when multidecadal variability was muted between 5000-3000 BP (Fig. S6). This is consistent with recent results from a California speleothem, which indicates that climate "whiplash" events (swings between wet and dry) were linked to biomass burning during the early Holocene (Homann et al. 2022).

4.3.4 The ecological consequences of Mazama ash deposition

The eruption of Mount Mazama (7627 +-150 yr BP, Egan et al. 2015) blanketed ash across 1.7 million km^2 of western North America (Egan et al. 2015). This abrupt landscape disturbance provides the opportunity to study the long-term response of ecosystems to short-term disruptions (Buma et al. 2019). Near the site of the eruption in high-altitude central Oregon, the ash destroyed understory vegetation, causing herbaceous pollen accumulation rates to decrease immediately after deposition (Long et al. 2014). Sites elsewhere in the Upper Columbia River Basin, Mack et al. (1979, 1978 a-c, 1976) also show post-Mazama increases in *Artemisia* at the expense of *Pinus*. Further away from the eruption, Schiller et al. (2020) examined a series of high-resolution pollen records from the Yellowstone area and showed an increase in *Artemisia* on the landscape for several centuries after the deposition of the tephra. At Round Lake, an increase in *Artemisia* pollen and a decline in *Pinus* pollen overlie the Mazama ash deposition (Fig. 9). The Mazama ash is depleted in nitrogen, phosphorous, and sulfur, creating a relatively infertile substrate for new growth (Geist and Cochran 1991, McDaniel et al. 2005, Schiller et al. 2020). Mulching may also have been responsible for the immediate expansion of *Artemisia* in the interior PNW*;* fine-grained Mazama-rich soils retain up to 100% more moisture, favorable for steppe species such as *Artemisia tridentata* (McDaniel et al. 2005). Steinman et al. (2019) conclude that a large positive isotope excursion in the Castor Lake $\delta^{18}O_{carbonate}$ record from the immediate post-Mazama period is a function of increased water retention on the landscape (and losses via evapotranspiration), consistent with this mulching effect (Fig. 9).

While the expansion of *Artemisia* in response to the Mazama ash lasted several centuries at other sites (Schiller et al. 2020), steppe-like vegetation persisted at Round Lake for millennia. Canonical correspondence analysis suggests that the landscape was richer than present in herbaceous taxa until 4600 BP (Fig. S8), more than three thousand years after the initial eruption. Two non-exclusive factors (in addition to the immediate edaphic effects of the tephra) may have contributed to the resilience of *Artemisia* on the landscape. First, $\delta^{18}O_{carbonate}$ values during this period indicate wet cool-seasons, but relatively dry summers with high fire activity preventing conifer expansion. In some sagebrush-dominated regions, wetter winter conditions, such as those indicated by the $\delta^{18}O_{carbonate}$ record, are associated with more surface fires given the increase in fine fuels (Miller and Tausch 2001). Elevated charcoal abundance and Hg accumulation rates after the Mazama support the idea that regional fire activity increased drastically after the ash deposition (Fig. 9). Frequent fires in sagebrush steppe-dry forest ecotones would have hindered the establishment of trees even when climatic and edaphic conditions were favorable to their growth (Mensing et al. 2006; Dugan and Baker 2015).

Second, increased multidecadal hydroclimate variability may have stalled the re-establishment of *Pinus* on the landscape. Intense, cyclic shifts between wet and dry periods became a prominent feature of the Round Lake $\delta^{18}O_{carbonate}$ record after the deposition of Mazama ash (Fig. 7, Fig. 9). Gray et al. (2006) showed that periodic, decadal-scale megadroughts during the 13th and 14th centuries in northeastern Utah limited conifer expansion and changed the structure of terrestrial ecosystems across large spatial scales. Additionally, the amplitude of multidecadal wet/dry cycles would have enhanced fire activity (Heyerdahl et al. 2008, Fig. S7), further hindering the expansion of arboreal vegetation.

The edaphic effect of the tephra represents a non-climatological complication which may explain the persistence of *Artemisia* on the landscape. The abrupt decrease in arboreal vegetation may have increased runoff and decreased evapotranspiration in the watershed which would have made the $\delta^{18}O_{carbonate}$ record more depleted without a true shift in regional climate. Forest clearance has previously been shown to make $\delta^{18}O_{carbonate}$ values more negative (Rosenmeier et al. 2002). The decline in $\delta^{18}O_{carbonate}$ values is protracted, rather than an immediate transition as seen in the pollen spectra, making this mechanism unlikely as a primary driver of the $\delta^{18}O_{carbonate}$ signal. Steinman et al. (2019) document the opposite isotopic signal at Castor Lake, owing to the increased water retention capacity of watershed soils after the tephra deposition, a response that apparently did not occur at Round Lake. The isotopic response of individual catchments to tephra deposition are likely sensitive to initial conditions such as the gradient (which can influence how deep and stable the resultant tephra is) and the initial vegetative cover (which would influence ecosystem response and recovery). Further study is necessary to more precisely understand how specific watersheds are likely to fare in the aftermath of such disturbances. It is therefore not obvious that the decrease in arboreal vegetation at Round Lake produced a depleted signal in the $\delta^{18}O_{carbonate}$ record. Ecosystem resilience clearly plays an important stabilizing role for millennia after the initial shift in the wake of a dramatic disturbance event.

Conclusions

High-resolution multiproxy analysis from Round Lake in the interior PNW sheds light on the coevolution of regional hydroclimate and ecology over the course of the Holocene. Stratigraphic indicators and oxygen isotopes suggest that the early Holocene (11,000-8200 BP) was marked by persistent aridity due to reduced cold-season precipitation and highly evaporative warm-seasons driven in part by elevated summer insolation. During the middle Holocene (8200-5300 BP), oxygen isotopes suggest increased winter precipitation, while the lithostratigraphy indicates intermediate and variable lake levels. Marine sedimentary records indicate persistently La Niña/PDO- like conditions in the middle Holocene, which would have directed winter storm tracks towards Round Lake. Summer insolation, however, remained higher than present and led to increased evapotranspiration. Late Holocene (5300 BP-present) stratigraphy suggests persistently high lake levels, while oxygen isotopes indicate a slight decline in cool-season precipitation, consistent with the record from nearby Castor Lake (Nelson et al. 2011, Lehmann et al. 2021).

Superimposed on these millennial-scale trends, ENSO- and PDO- scale variability have played important roles in the hydroclimatic history of the PNW. At both Round Lake and nearby Castor Lake, climate variability on the order of 10-100 years is muted during the early Holocene. Both lake records began to show statistically significant periodicities in the 16-32 year band at approximately 7000 BP. Between 5000-3000 BP, significant periodicities at both sites persist only at lower (~64 year) frequencies, and the past millennium contains the highest amplitude of cycles between wet and dry periods of the entire Holocene. These trends closely match reconstructed ENSO strength from coral $\delta^{18}O$ records in the tropical Pacific. When ENSO amplitude is high, PDO-scale variability is prominent at Castor and Round lakes.

Millennial- to decadal-scale climate variability have driven ecosystem dynamics in the region since deglaciation. Many records indicate largely steppe-like conditions, rich in Poaceae and *Artemisia* during the arid early Holocene. Despite this, charcoal abundance, microcharcoal percentage, and Hg accumulation rates are relatively low, reflecting low-severity high-frequency surface fires. During the middle Holocene, conifer forest expanded, and fire activity was higher than the early Holocene, as cool-season moisture increased and summer insolation remained high. Modern forest communities emerged by approximately 4600 BP, when conditions were wetter than before. Conifer expansion, however, lagged behind the climate drivers by several decades; whereas steppe taxa (e.g., *Artemisia* and Poaceae), lack any clear relationship to antecedent hydroclimate conditions. As moisture availability is anticipated to decrease and hydroclimate variability expected to increase in the coming centuries, (Mote and Salathe 2010), herbaceous vegetation may fare better than slower-growing, more moisture sensitive arboreal species under future warming scenarios. Fire activity was sensitive to the amplitude of multidecadal climate forcing. The increased amplitude of wet/dry cycles led to abundant fine-fuel production during multidecadal wet periods that subsequently desiccated and burned during dry periods. The deposition of Mazama ash on the landscape was an important non-climatic driver of ecosystem change in the interior Northwest. Despite relatively high cool-season precipitation in the millennia following the eruption, pollen assemblages indicate a persistence of steppe vegetation at that time, due to changes in soil characteristics, highly evaporative summer conditions, multidecadal droughts, and/or increased fire activity.

This study highlights the value of coupling hydroclimate and ecological proxy data from the same sedimentary sequence. Additionally, sub-decadal temporal resolution of proxy data can help elucidate changes in the climate system which otherwise remain obscure. This approach can provide valuable context for understanding climate extremes and decadal variability in the future.

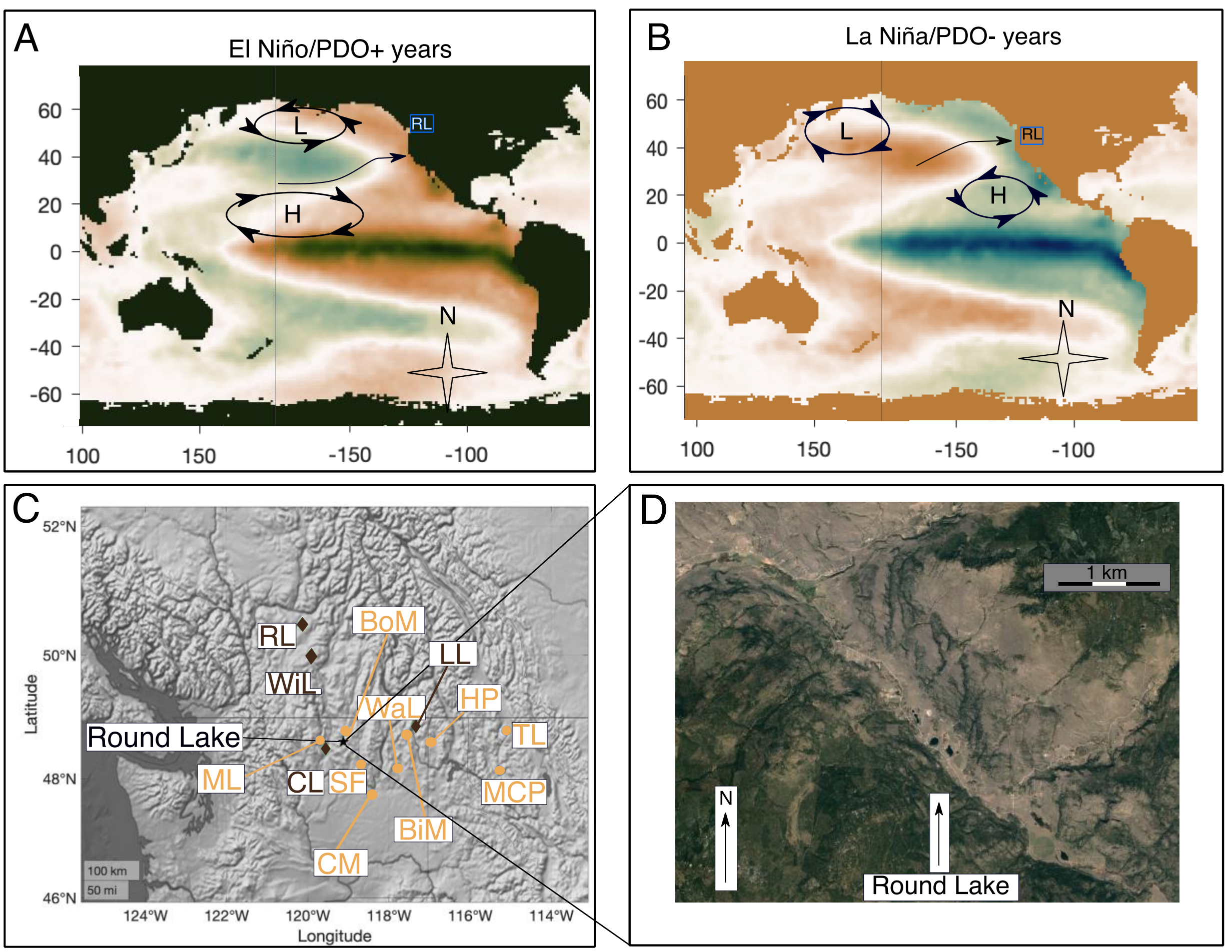

Fig. 1: (A) The impact of El Niño/PDO+ conditions on prevailing pressure systems (circular arrows) and stormtracks (black arrows) in the mid-latitude eastern Pacific. Study site (Round Lake) represented in blue circle. Warm colors indicate warm temperature anomalies, while

cooler colors suggest cool anomalies. (B) Same as in (A) but for La Niña/PDO- conditions. (C) Location of different proxy sites discussed in the text. Orange circles represent pollen sites from Fig. S6, from E to W: TL=Tepee Lake MCP=McKillop Creek Pond HP=Hagar Pond BiM=Big Meadows WaL=Waits Lake CM=Creston Mire BoM=Bonaparte Meadows ML=Mud Lake. Maroon diamonds indicate other reconstructions plotted in Fig. 6, from E to W: LL=Lime Lake CL=Castor Lake WiL=Windy Lake RL=Roche Lake. Round Lake is the black star. (D) Aerial image of the Round Lake watershed.

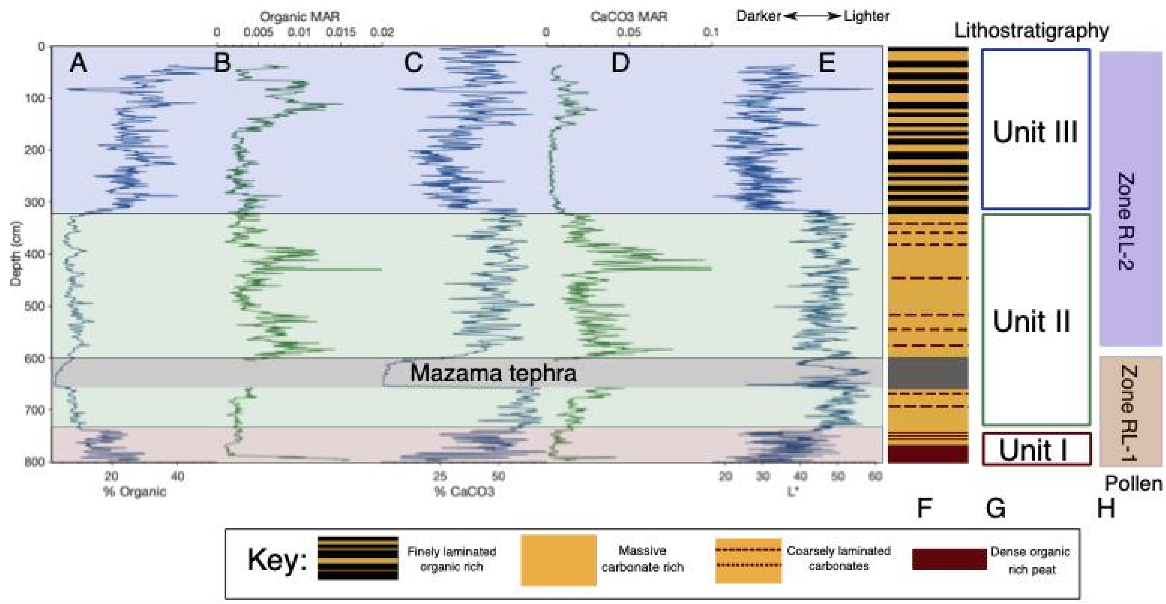

Fig. 2: Physical sedimentology data for Round Lake A-17 and B-18. (L to R) (A) % organic matter (B) organic matter mass accumulation rate (MAR, $g/cm^2/yr$) (C) % calcium carbonate ($CaCO_3$) (D) $CaCO_3$ mass accumulation rate (MAR $g/cm^2/yr$) (E) L* perceptual lightness (F) core schematic (see bottom for key) (G) major lithologic units and (H) pollen zones. X-axes for organic matter and $CaCO_3$ MAR have been clipped to emphasize variability and do not show maximum values.

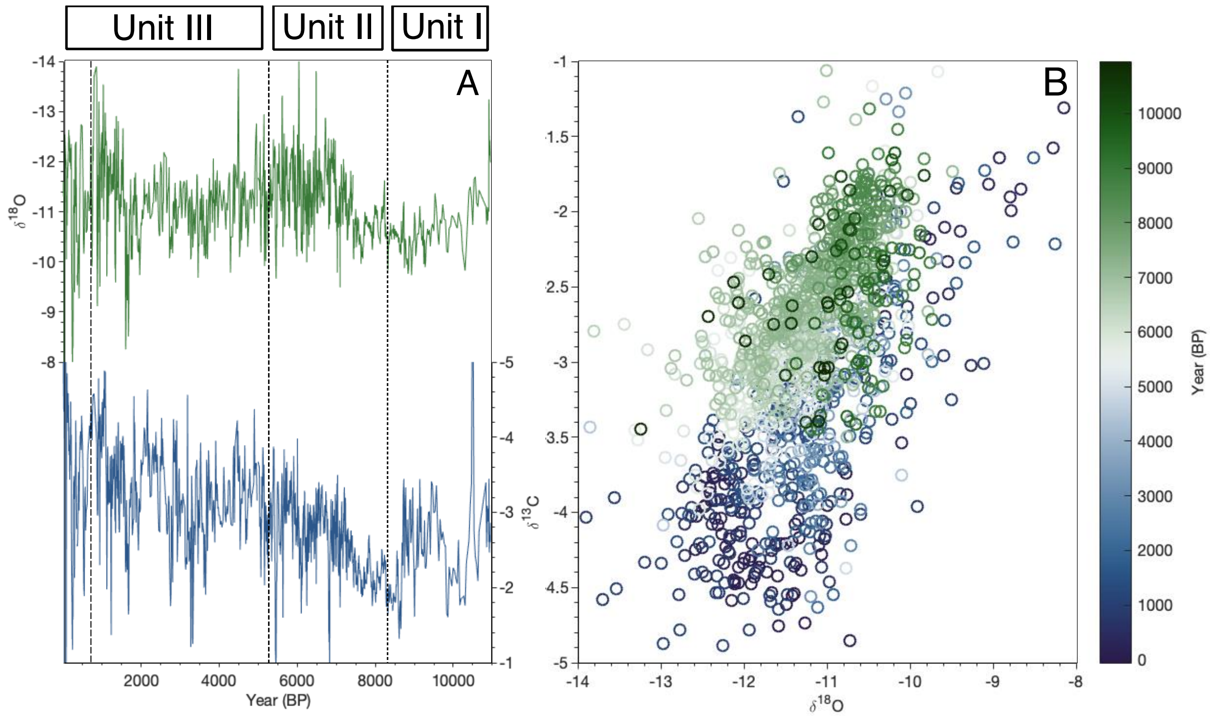

Fig. 3: Carbonate isotopic results from Round Lake Core A-17 and Round Lake Core B-18 (A) ^{18}O (green) and ^{13}C (blue) time series. (B) Scatter plot of ^{18}O and ^{13}C. Color for each data point represents age BP (see color bar).

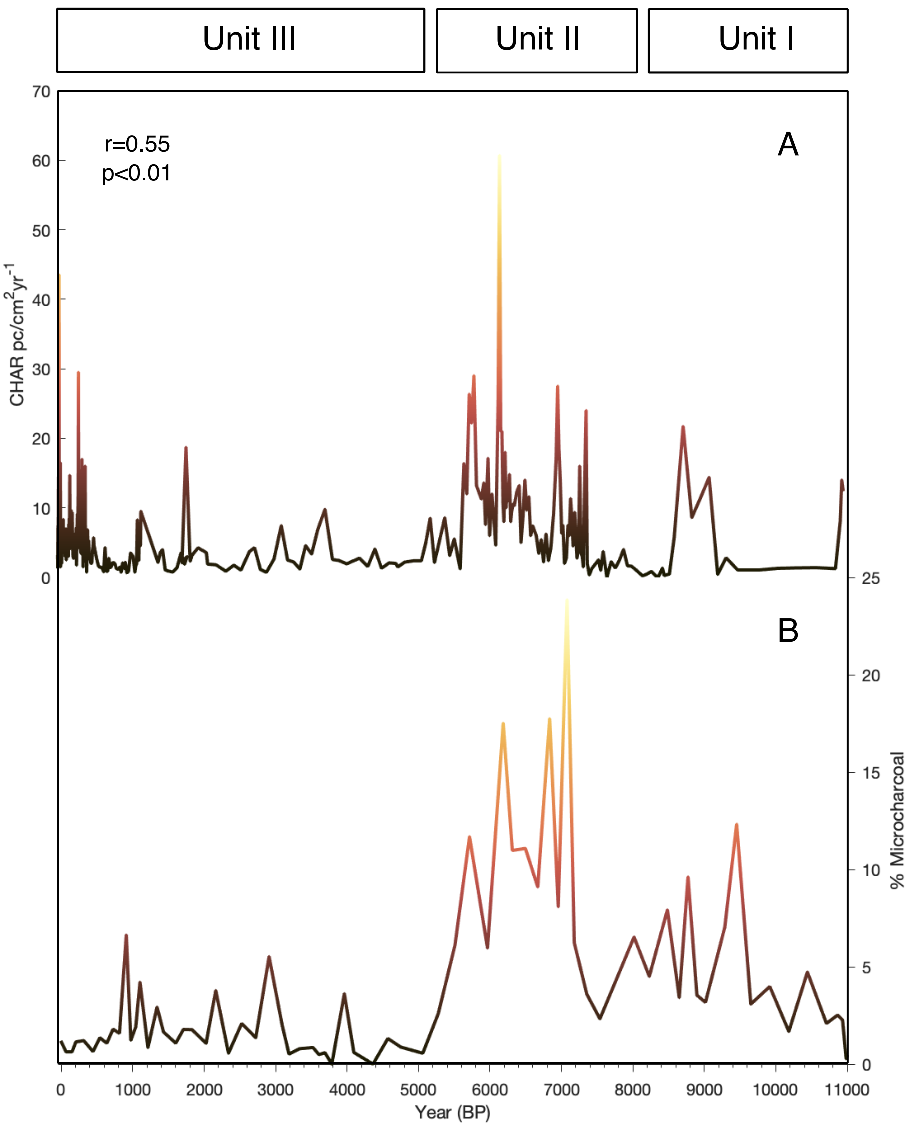

Fig. 4: Charcoal accumulation rate (>125-μm CHAR; A) and micro-charcoal percentages (B) from Round Lake. Correlation coefficient (r=0.55) and p-values (after accounting for autocorrelation) for the two time-series are indicated in A.

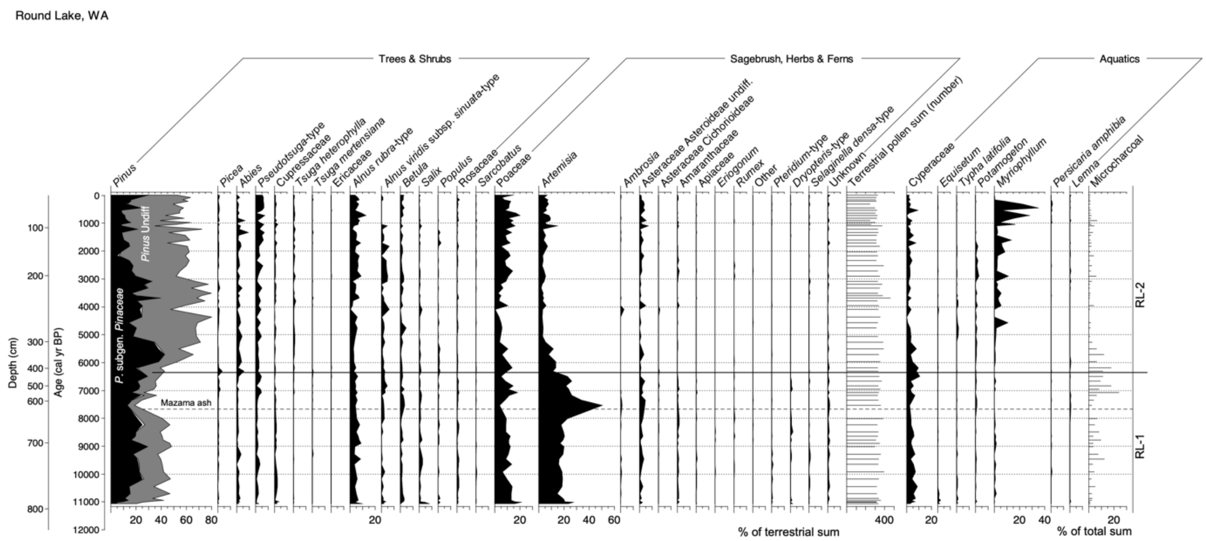

Fig. 5: Round Lake pollen percentages and charcoal flux, plotted as both age (BP, interior y-axis) and depth (cm, exterior y axis). Dashed horizontal line represents Mazama tephra layer.

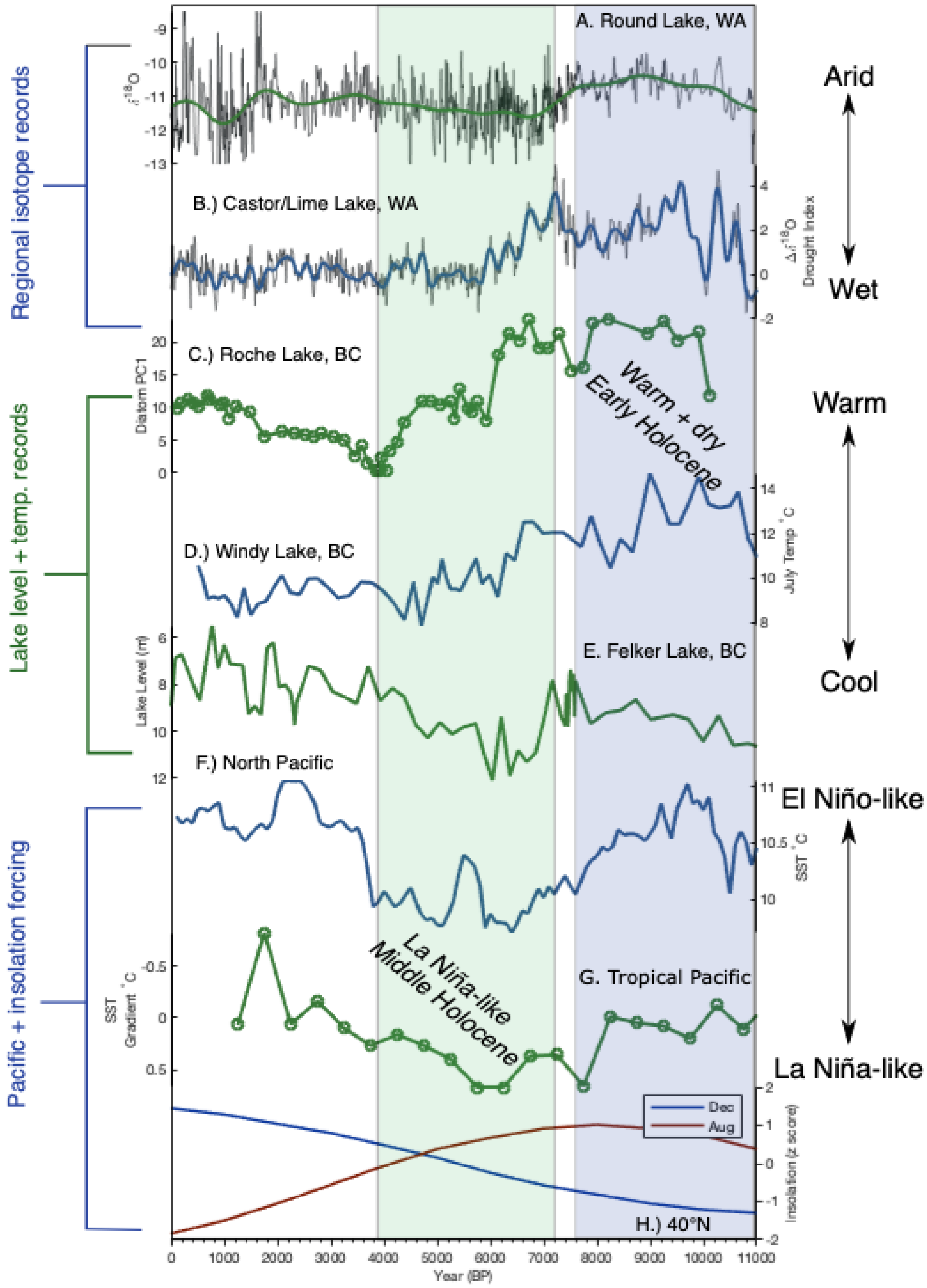

Fig. 6: Summary of proxy reconstructions and potential forcing mechanisms (top to bottom): (A) Round Lake $\delta^{18}O$, (B) Castor-Lime Lake drought index reconstruction (Lehmann et al. 2021), (C) PC1 of diatom abundances indicating lake level history from Roche Lake (Mushet et al. 2022), (D) Windy Lake chironomid based July temperature reconstruction (Chase et al. 2008),

(E) Felker Lake diatom-inferred lake level reconstruction (Galloway et al. 2011) (F) North Pacific sea-surface temperature reconstruction (Praetorius et al. 2020), (G) east-west tropical SST gradient (Koutavas and Joanides, 2012) and (H) Dec/Aug insolation anomalies at 40 N latitude.

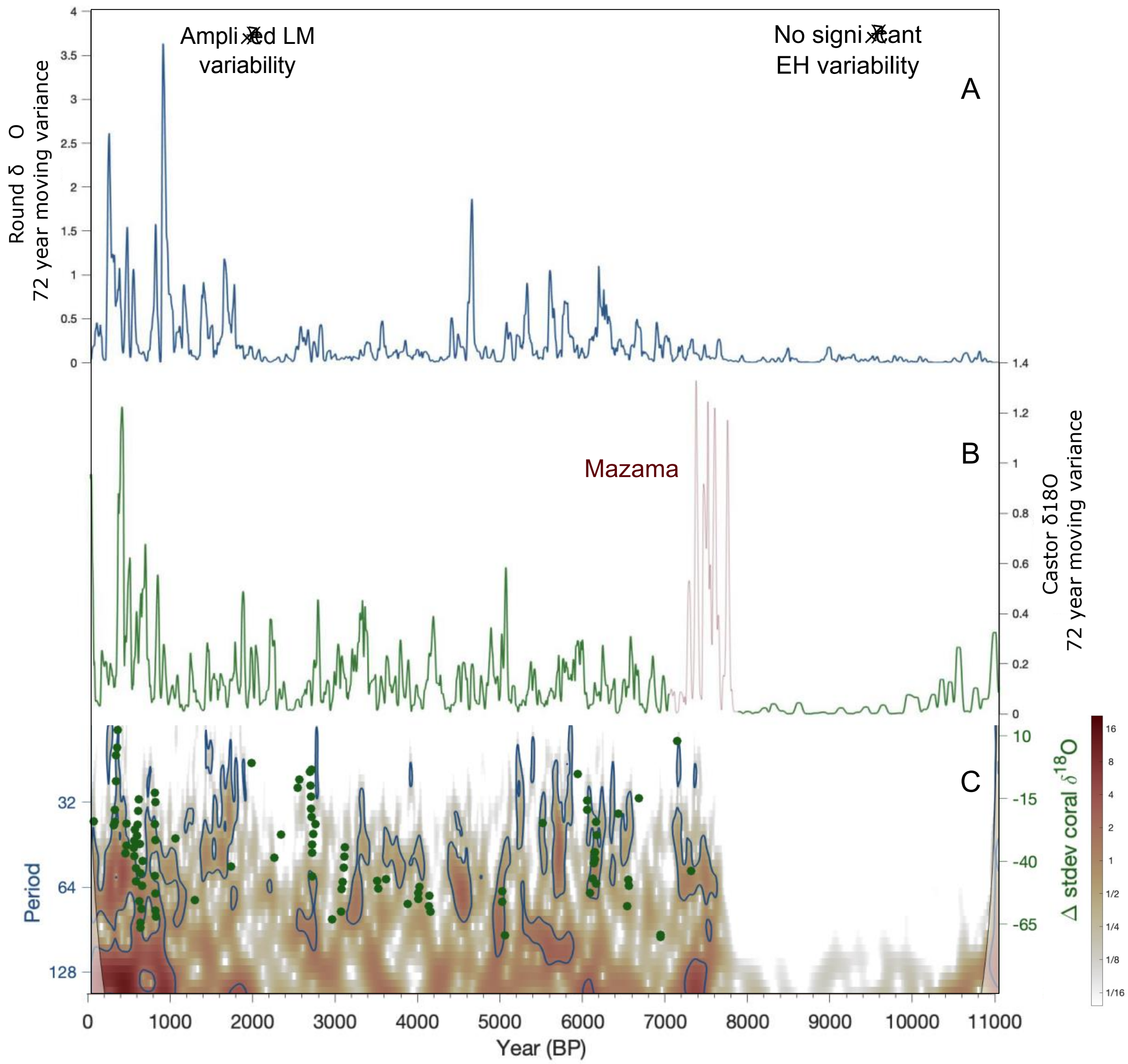

Fig. 7: 72-year moving variance in $\delta^{18}O_{carbonate}$ records from (A) Round (B) Castor lakes. Thin red line in Castor Lake record covers the period immediately following the Mazama tephra deposition, which created enriched oxygen isotope values for several centuries afterward (see Steinman et al. 2019). (C) Cross-wavelet between Castor and Round Lake $\delta^{18}O_{carbonate}$ record. Blue line indicates shared periodicities which are significant at a 95% confidence interval based

on AR1 model. Green dots indicate changes in the standard deviation of tropical Pacific coral $\delta^{18}O_{carbonate}$ composite (Grothe et al. 2020), reflecting ENSO amplitude.

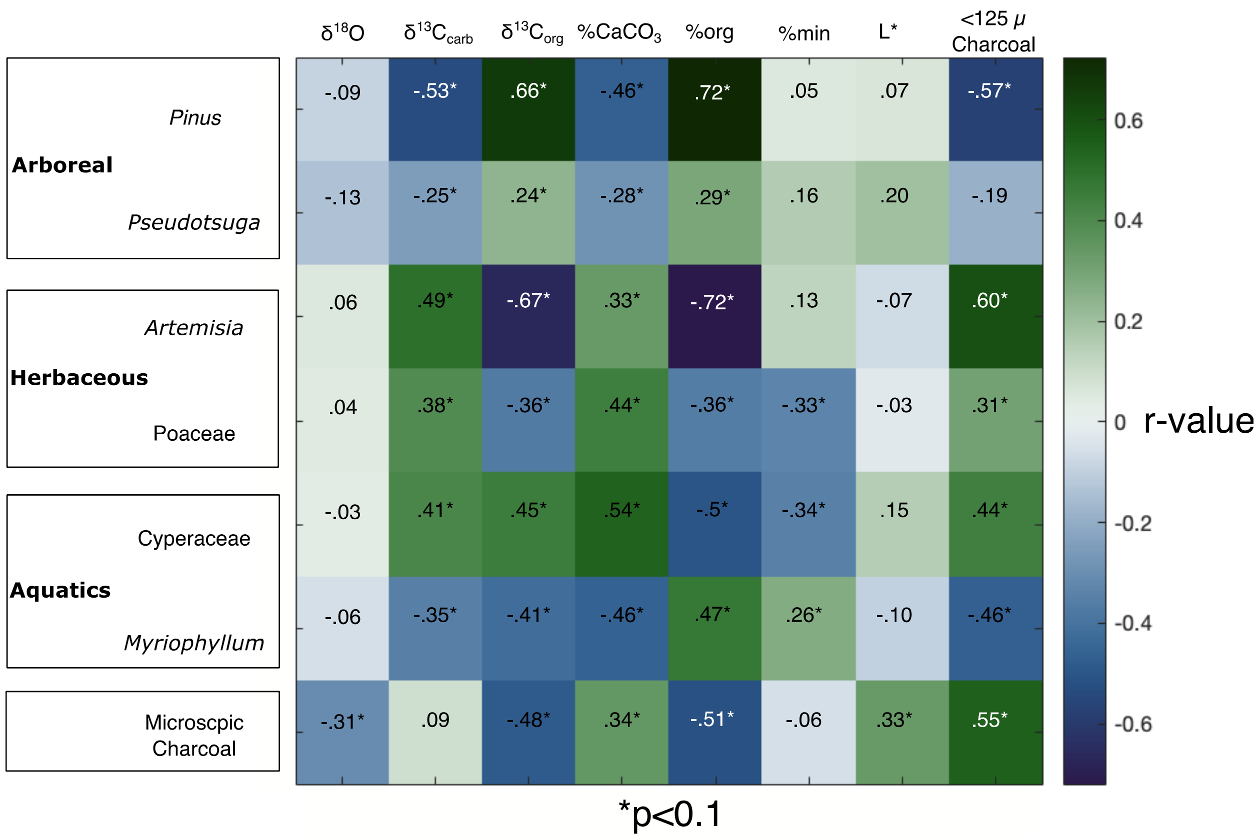

Fig. 8: Correlation matrix of Round Lake multiproxy data and pollen counts. Shading of each box represents the r value. Number in each box represents the r value of each proxy combination.

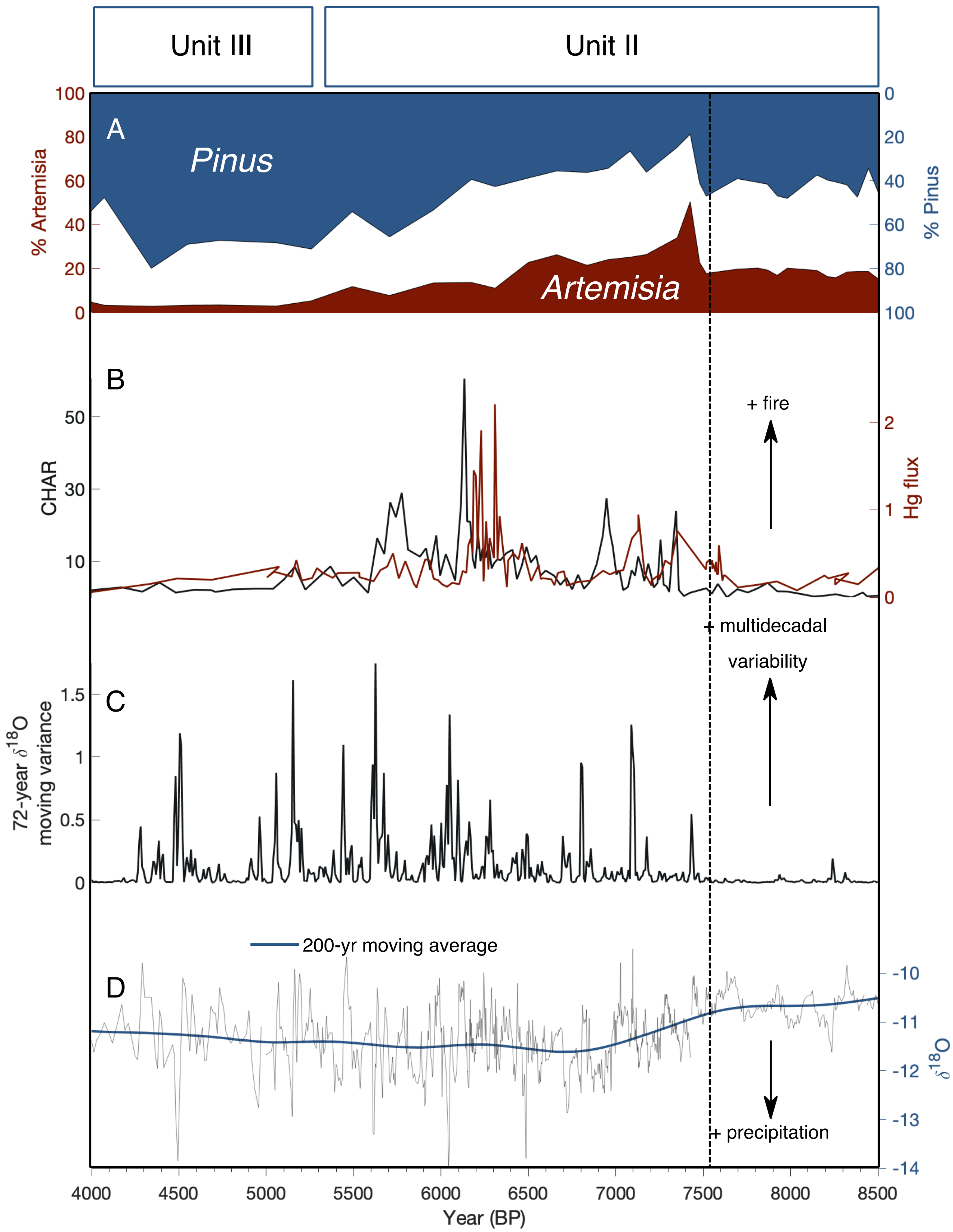

Fig. 9 (A) *Artemisia* and *Pinus* percentages (B) CHAR and Hg concentration (C) multidecadal hydroclimate variability and (d) $\delta^{18}O$ from Round Lake (blue line is raw data, green line indicates

200-year loess smoothing filter) during immediately before and after the deposition of the Mazama tephra (vertical dashed line).

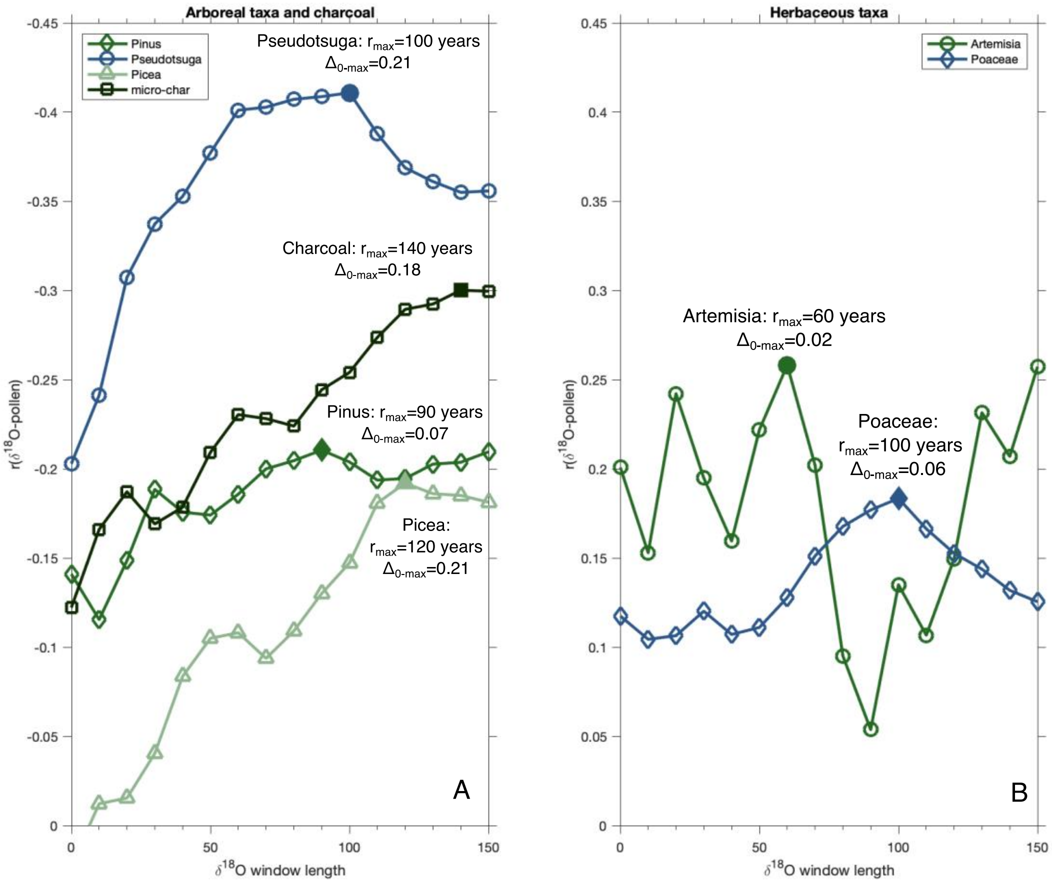

Fig. 10: Correlation between Round Lake $\delta^{18}O$ values with different preceding window lengths (see Fig. S10 for illustration of method) and different (A) arboreal and charcoal and (B) herbaceous/grass pollen types. Solid shape indicate the window length with the highest r value.

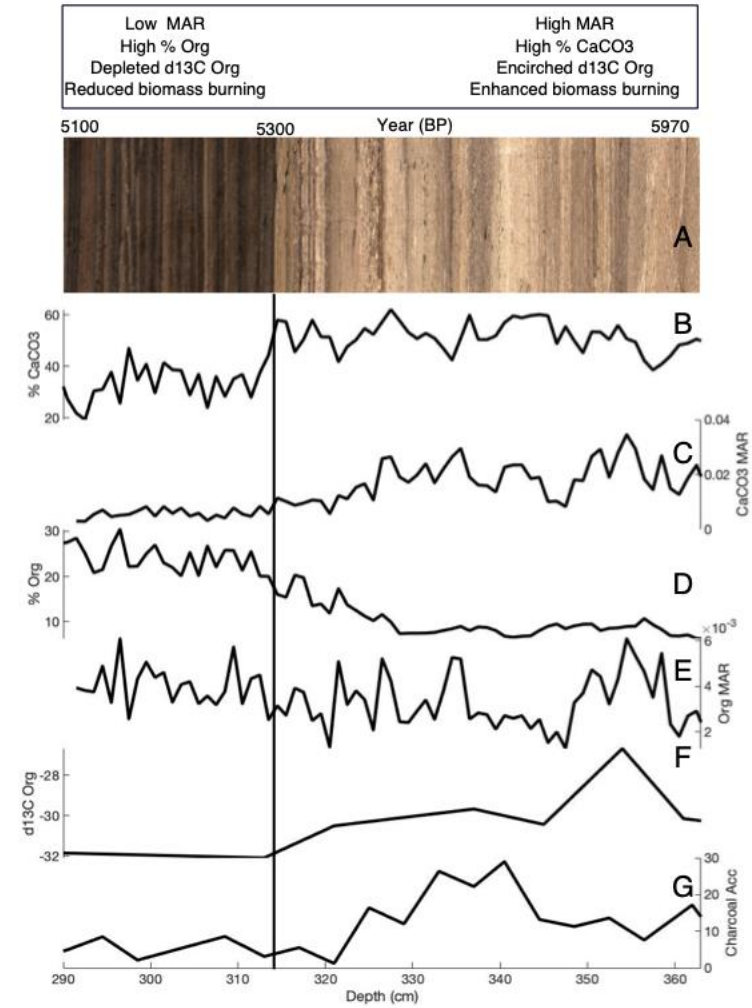

Fig. S1: The abrupt transition between light colored carbonate rich sediments of the middle Holocene and dark, finely laminated sediments of the late Holocene, with several proxies across this boundary. (A) Core image illustrating abrupt transition (B) %$CaCO_3$ (C) $CaCO_3$ mass accumulation rate (MAR) (D) Percent organic matter (E) Organic matter mass accumulation rate (MAR ($g/cm^2/yr$) (F) $\delta^{13}C$ of organic matter (G) Charcoal accumulation rate. Chronological information is presented above (A).

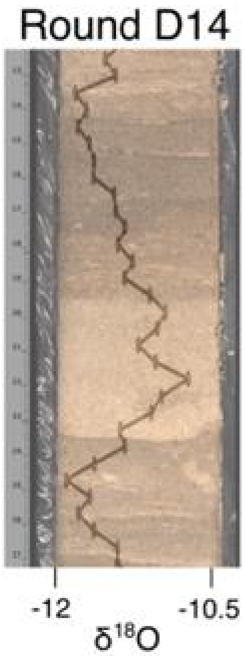

Fig. S2: Representative Unit II stratigraphy with oxygen isotopes overlain.

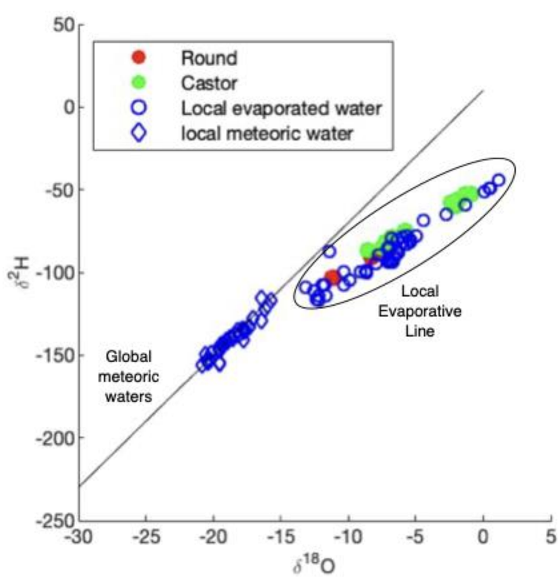

Fig. S3: Oxygen and hydrogen isotope composition of global and local meteoric and evaporative waters. Castor Lake (green dots) and Round Lake (red dots) water samples were taken between 2000 and 2018 (taken from Mark et al. 2023).

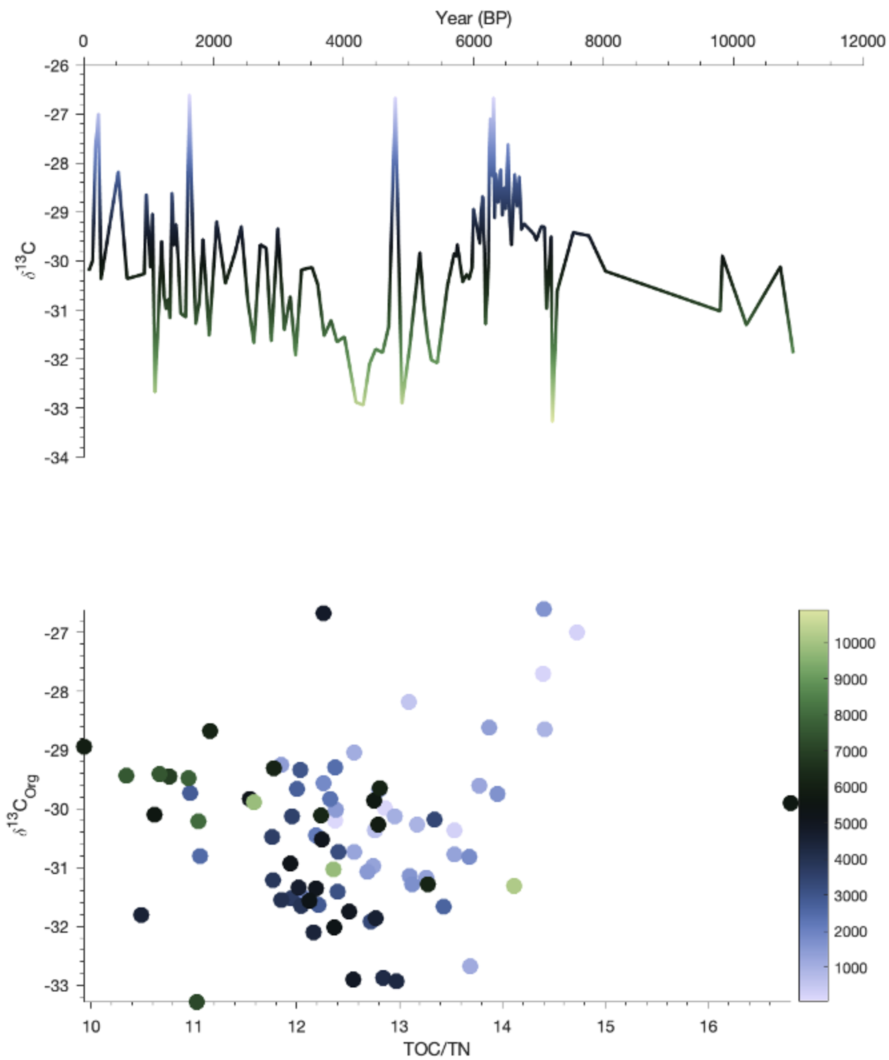

Fig. S4: Top: $\delta^{113}C_{organic}$ time series from Round Lake. Bottom: Scatter plot of organic ^{13}C isotopes and TOC/TN. Color of each data point represents age BP (see color bar).

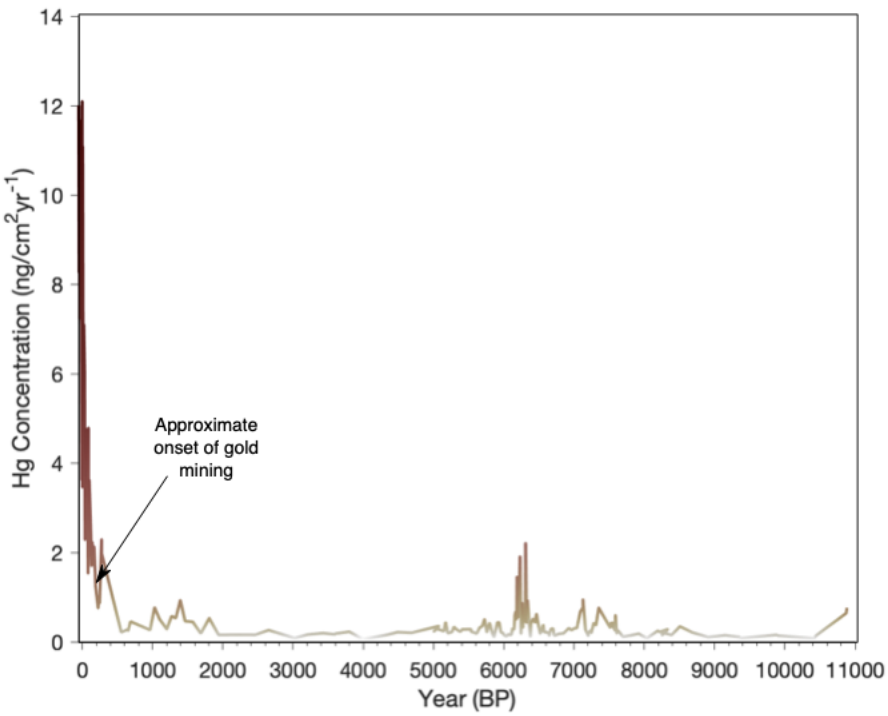

Fig. S5: Full Holocene record of Round Lake mercury accumulation.

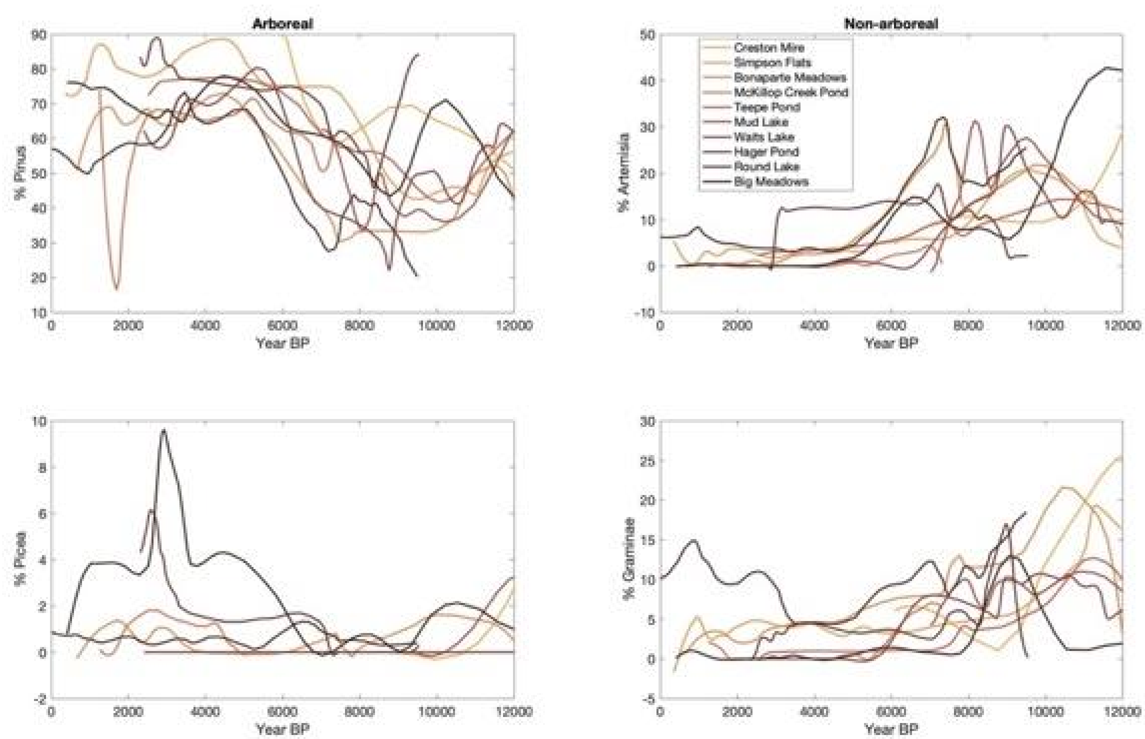

Fig. S6: Pollen percentages of common arboreal and non-arboreal taxa from lakes in northwestern North America including: Mud Lake (Mack et al. 1979), Round Lake (this study), Bonaparte Meadows (Mack et al. 1979), Simpson's Flats (Mack et al. 1978a), Creston Mire (Mack et al. 1976), Waits Lake (Mack et al. 1978b), Big Meadows (Mack et al. 1978c), Hager Pond (Mack et al. 1978c), McKillop Creek Pond (Mack et al. 1983), and Tepee Lake (Mack et al. 1983).

Acknowledgements:

This research was funded by NSF Grant #1446283 and by the Andrew Mellon Predoctoral Fellowship at the University of Pittsburgh. The authors thank Drs. Molly O'Beirne, Elliot Arnold, and Josef Werne for laboratory assistance and Dr. Benjamin Gaglioti for discussion of the manuscript.

References Cited:

Alexander, M. A., et al. (2002). "The atmospheric bridge: The influence of ENSO teleconnections on air–sea interaction over the global oceans." Journal of climate **15**(16): 2205-2231.

Alt, M., et al. (2018). "Millennial scale climate-fire-vegetation interactions in a mid-elevation mixed coniferous forest, Mission Range, northwestern Montana, USA." Quaternary Research **90**(1): 66-82.

Anderson, L., et al. (2005). "Regional atmospheric circulation change in the North Pacific during the Holocene inferred from lacustrine carbonate oxygen isotopes, Yukon Territory, Canada." Quaternary Research **64**(1): 21-35.

Arno, S. F., et al. (2000). Mixed-severity fire regimes in the northern Rocky Mountains: consequences of fire exclusion and options for the future. Wilderness science in a time of change conference, Rocky Mountain Research Station Ogden, UT.

Barron, J. A. and L. Anderson (2011). "Enhanced Late Holocene ENSO/PDO expression along the margins of the eastern North Pacific." Quaternary International **235**(1-2): 3-12.

Bartlein, P. J., et al. (1998). "Paleoclimate simulations for North America over the past 21,000 years: features of the simulated climate and comparisons with paleoenvironmental data." Quaternary Science Reviews **17**(6-7): 549-585.

Bartlein, P. J., et al. (2014). "Paleoclimate." Climate Change in North America: 1-51.

Bennett, K. D. and K. J. Willis (2001). "Pollen." Tracking environmental change using lake sediments: terrestrial, algal, and siliceous indicators: 5-32.

Besonen, M. R., et al. (2008). "A record of climate over the last millennium based on varved lake sediments from the Canadian High Arctic." The Holocene **18**(1): 169-180.

Bretherton, C. S., et al. (1999). "The effective number of spatial degrees of freedom of a time-varying field." Journal of climate **12**(7): 1990-2009.

Brown, K. J. and R. J. Hebda (2002). "Origin, development, and dynamics of coastal temperate conifer rainforests of southern Vancouver Island, Canada." Canadian journal of forest research **32**(2): 353-372.

Brunelle, A. and C. Whitlock (2003). "Postglacial fire, vegetation, and climate history in the Clearwater Range, Northern Idaho, USA." Quaternary Research **60**(3): 307-318.

Bryson, R. A. and F. K. Hare (1974). "Climates of North America." (No Title).

Buma, B., et al. (2019). "The value of linking paleoecological and neoecological perspectives to understand spatially-explicit ecosystem resilience." Landscape Ecology **34**(1): 17-33.

Chase, M., et al. (2008). "Midge-inferred Holocene summer temperatures in southeastern British Columbia, Canada." Palaeogeography, Palaeoclimatology, Palaeoecology **257**(1-2): 244-259.

Cobb, K. M., et al. (2013). "Highly variable El Niño–southern oscillation throughout the Holocene." Science **339**(6115): 67-70.

Cook, E. R., et al. (2004). "Long-term aridity changes in the western United States." Science **306**(5698): 1015-1018.

Cooper, C. S., et al. (2021). "A lake sediment–based paleoecological reconstruction of late Holocene fire history and vegetation change in Great Basin National Park, Nevada, USA." Quaternary Research **104**: 28-42.

Crameri, F. (2018). "Scientific colour maps." Zenodo **10**.

Dean, W. E. (1999). "The carbon cycle and biogeochemical dynamics in lake sediments." Journal of Paleolimnology **21**: 375-393.

Diffenbaugh, N. S., et al. (2006). "Summer aridity in the United States: Response to mid-Holocene changes in insolation and sea surface temperature." Geophysical Research Letters **33**(22).

Du, X., et al. (2021). "High-resolution interannual precipitation reconstruction of Southern California: Implications for Holocene ENSO evolution." Earth and Planetary Science Letters **554**: 116670.

Dugan, A. J. and W. L. Baker (2015). "Sequentially contingent fires, droughts and pluvials structured a historical dry forest landscape and suggest future contingencies." Journal of Vegetation Science **26**(4): 697-710.

Eagles-Smith, C. A., et al. (2018). "Modulators of mercury risk to wildlife and humans in the context of rapid global change." Ambio **47**: 170-197.

Egan, J., et al. (2015). "A high-precision age estimate of the Holocene Plinian eruption of Mount Mazama, Oregon, USA." The Holocene **25**(7): 1054-1067.

Emile-Geay, J., et al. (2016). "Links between tropical Pacific seasonal, interannual and orbital variability during the Holocene." Nature Geoscience **9**(2): 168-173.

Esdaile, L. J. and J. M. Chalker (2018). "The mercury problem in artisanal and small- scale gold mining." Chemistry–A European Journal **24**(27): 6905-6916.

Fox Jr, K. F. (1970). Geologic map of the Oroville quadrangle, Okanogan County, Washington.

Galloway, J. M., et al. (2011). "Hydrological change in the central interior of British Columbia, Canada: diatom and pollen evidence of millennial-to-centennial scale change over the Holocene." Journal of Paleolimnology **45**: 183-197.

Geist, J. and P. Cochran (1991). "Influences of volcanic ash and pumice deposition on productivity of western interior forest soils." Harvey, AE, Neuenschwander, LF (Compilers), Proc., Management and Productivity of Western-Montane Forest Soils. USDA For. Serv. Gen. Tech. Rep. INT-280, Ogden, UT: 82-88.

Gherardi, L. A. and O. E. Sala (2015). "Enhanced precipitation variability decreases grass-and increases shrub-productivity." Proceedings of the National Academy of Sciences **112**(41): 12735-12740.

Gray, S. T., et al. (2006). "Role of multidecadal climate variability in a range extension of pinyon pine." Ecology **87**(5): 1124-1130.

Grimm, E. C. (1987). "CONISS: a FORTRAN 77 program for stratigraphically constrained cluster analysis by the method of incremental sum of squares." Computers & geosciences **13**(1): 13-35.

Grinsted, A., et al. (2004). "Application of the cross wavelet transform and wavelet coherence to geophysical time series." Nonlinear processes in geophysics **11**(5/6): 561-566.

Grothe, P. R., et al. (2020). "Enhanced El Niño–Southern oscillation variability in recent decades." Geophysical Research Letters **47**(7): e2019GL083906.

Hebda, R. J. (1995). "British Columbia vegetation and climate history with focus on 6 ka BP." Géographie physique et Quaternaire **49**(1): 55-79.

Heiri, O., et al. (2001). "Loss on ignition as a method for estimating organic and carbonate content in sediments: reproducibility and comparability of results." Journal of Paleolimnology **25**: 101-110.

Helmer, M., et al. (2020). "Mapping heritage ecosystem services in ecological restoration areas: A case study from the East Cascades, Washington." Journal of Outdoor Recreation and Tourism **31**: 100314.

Hessl, A. E., et al. (2004). "Drought and Pacific Decadal Oscillation linked to fire occurrence in the inland Pacific Northwest." Ecological applications **14**(2): 425-442.

Heyerdahl, E. K., et al. (2008). "Climate drivers of regionally synchronous fires in the inland Northwest (1651–1900)." International Journal of Wildland Fire **17**(1): 40-49.

Higuera, P. E. and J. T. Abatzoglou (2021). "Record- setting climate enabled the extraordinary 2020 fire season in the western United States." Global change biology **27**(1).

Hillman, A. L., et al. (2018). "Climate and anthropogenic controls on the carbon cycle of Xingyun Lake, China." Palaeogeography, Palaeoclimatology, Palaeoecology **501**: 70-81.

Hodell, D. A. and C. L. Schelske (1998). "Production, sedimentation, and isotopic composition of organic matter in Lake Ontario." Limnology and Oceanography **43**(2): 200-214.

Homann, J., et al. (2022). "Linked fire activity and climate whiplash in California during the early Holocene." Nature Communications **13**(1): 7175.

Horton, T. W., et al. (2016). "Evaporation induced 18O and 13C enrichment in lake systems: A global perspective on hydrologic balance effects." Quaternary Science Reviews **131**: 365-379.

Jain, T. B., et al. (2012). "A comprehensive guide to fuel management practices for dry mixed conifer forests in the northwestern United States."

Komada, T., et al. (2008). "Carbonate removal from coastal sediments for the determination of organic carbon and its isotopic signatures, δ13C and Δ14C: comparison of fumigation and direct acidification by hydrochloric acid." Limnology and Oceanography: Methods **6**(6): 254-262.

Koutavas, A. and S. Joanides (2012). "El Niño–Southern oscillation extrema in the holocene and last glacial maximum." Paleoceanography **27**(4).

Kovanen, D. J. and O. Slaymaker (2004). "Glacial imprints of the Okanogan Lobe, southern margin of the Cordilleran Ice Sheet." Journal of Quaternary Science: Published for the Quaternary Research Association **19**(6): 547-565.

Lasher, G. E., et al. (2021). "Holocene hydroclimatic reorganizations in northwest Canada inferred from lacustrine carbonate oxygen isotopes." Geophysical Research Letters **48**(16): e2021GL092948.

Lehmann, S. B., et al. (2021). "Prolonged early to middle Holocene drought in the Pacific Northwest inferred from lacustrine carbonate oxygen isotope values and sedimentology." Quaternary Science Reviews **271**: 107192.

Li, H.-C. and T.-L. Ku (1997). "δ13C–δ18C covariance as a paleohydrological indicator for closed-basin lakes." Palaeogeography, Palaeoclimatology, Palaeoecology **133**(1-2): 69-80.

Long, C. J., et al. (2014). "The impact of Mt Mazama tephra deposition on forest vegetation in the Central Cascades, Oregon, USA." The Holocene **24**(4): 503-511.

Mack, R. N., et al. (1976). "Pollen sequence from the Columbia Basin, Washington: Reappraisal of postglacial vegetation." American Midland Naturalist: 390-397.

Mack, R. N., et al. (1978). "Late Quaternary pollen record from Big Meadow, Pend Oreille County, Washington." Ecology **59**(5): 956-965.

Mack, R. N., et al. (1978). "Late Quaternary pollen record from the Sanpoil River valley, Washington." Canadian Journal of Botany **56**(14): 1642-1650.

Mack, R. N., et al. (1979). "Holocene vegetation history of the Okanogan Valley, Washington." Quaternary Research **12**(2): 212-225.

Mack, R. N., et al. (1983). "Holocene vegetational history of the Kootenai River valley, Montana." Quaternary Research **20**(2): 177-193.

Mann, M. E., et al. (2021). "Multidecadal climate oscillations during the past millennium driven by volcanic forcing." Science **371**(6533): 1014-1019.

Mark, S. Z., et al. (2022). "XRF analysis of Laguna Pallcacocha sediments yields new insights into Holocene El Niño development." Earth and Planetary Science Letters **593**: 117657.

McAfee, S. A. and E. K. Wise (2016). "Intra- seasonal and inter- decadal variability in ENSO impacts on the Pacific Northwest." International Journal of Climatology **36**(1): 508-516.

McDaniel, P., et al. (2005). "Andic soils of the inland Pacific Northwest, USA: properties and ecological significance." Soil science **170**(4): 300-311.

Meko, D. M., et al. (2007). "Medieval drought in the upper Colorado River Basin." Geophysical Research Letters **34**(10).

Mensing, S., et al. (2006). "Long-term fire history in Great Basin sagebrush reconstructed from macroscopic charcoal in spring sediments, Newark Valley, Nevada." Western North American Naturalist **66**(1): 64-77.

Metcalfe, S. E., et al. (2015). "The Holocene history of the North American Monsoon:'known knowns' and 'known unknowns' in understanding its spatial and temporal complexity." Quaternary Science Reviews **120**: 1-27.

Meyers, P. A. and E. Lallier-Vergès (1999). "Lacustrine sedimentary organic matter records of Late Quaternary paleoclimates." Journal of Paleolimnology **21**: 345-372.

Miller, R. F. and R. J. Tausch (2000). The role of fire in pinyon and juniper woodlands: a descriptive analysis. Proceedings of the invasive species workshop: the role of fire in the control and spread of invasive species. Fire conference.

Millspaugh, S. H., et al. (2000). "Variations in fire frequency and climate over the past 17 000 yr in central Yellowstone National Park." Geology **28**(3): 211-214.

Mote, P. W. and E. P. Salathé Jr (2010). "Future climate in the Pacific Northwest." Climatic change **102**(1-2): 29-50.

Murton, D. K. and S. J. Crowhurst (2020). "Cross correlation of CIELAB color reflectance data from archive photographs and line-scan images of sediment." Quaternary Research **93**: 267-283.

Mushet, G. R., et al. (2022). "Postglacial hydroclimate in the southern interior of British Columbia (Canada): Lake ecosystem response to the Holocene Thermal Maximum and drivers of mid-to-late Holocene climate variability." Quaternary Science Reviews **276**: 107302.

Mustaphi, C. J. C. and M. F. Pisaric (2014). "A classification for macroscopic charcoal morphologies found in Holocene lacustrine sediments." Progress in Physical Geography **38**(6): 734-754.

Nelson, D. B., et al. (2011). "Drought variability in the Pacific Northwest from a 6,000-yr lake sediment record." Proceedings of the National Academy of Sciences **108**(10): 3870-3875.

Newman, M., et al. (2016). "The Pacific decadal oscillation, revisited." Journal of climate **29**(12): 4399-4427.

Parnell, A. (2014). "Bchron: Radiocarbon dating, age-depth modelling, relative sea level rate estimation, and non-parametric phase modelling." R package version **4**(1).

Pompeani, D. P., et al. (2018). "Climate, fire, and vegetation mediate mercury delivery to midlatitude lakes over the holocene." Environmental science & technology **52**(15): 8157-8164.

Praetorius, S. K., et al. (2020). "The role of Northeast Pacific meltwater events in deglacial climate change." Science advances **6**(9): eaay2915.

Reimer, P. J., et al. (2020). "The IntCal20 Northern Hemisphere radiocarbon age calibration curve (0–55 cal kBP)." Radiocarbon **62**(4): 725-757.

Rodionov, S., et al. (2007). "The Aleutian Low, storm tracks, and winter climate variability in the Bering Sea." Deep Sea Research Part II: Topical Studies in Oceanography **54**(23-26): 2560-2577.

Rosenmeier, M. F., et al. (2002). "A 4000-year lacustrine record of environmental change in the southern Maya lowlands, Petén, Guatemala." Quaternary Research **57**(2): 183-190.

Santos, G. M. and K. Ormsby (2013). "Behavioral variability in ABA chemical pretreatment close to the 14C age limit." Radiocarbon **55**(2): 534-544.

Schiller, C. M., et al. (2020). "Vegetation responses to Quaternary volcanic and hydrothermal disturbances in the Northern Rocky Mountains and Greater Yellowstone Ecosystem (USA)." Palaeogeography, Palaeoclimatology, Palaeoecology **559**: 109859.

Schnurrenberger, D., et al. (2003). "Classification of lacustrine sediments based on sedimentary components." Journal of Paleolimnology **29**: 141-154.

Shapley, M. D., et al. (2005). "Authigenic calcium carbonate flux in groundwater-controlled lakes: implications for lacustrine paleoclimate records." Geochimica et Cosmochimica Acta **69**(10): 2517-2533.

Shuman, B., et al. (2009). "Holocene lake-level trends in the Rocky Mountains, USA." Quaternary Science Reviews **28**(19-20): 1861-1879.

Shuman, B. N., et al. (2009). "Abrupt climate change as an important agent of ecological change in the Northeast US throughout the past 15,000 years." Quaternary Science Reviews **28**(17-18): 1693-1709.

Steinman, B. A. and M. B. Abbott (2013). "Isotopic and hydrologic responses of small, closed lakes to climate variability: Hydroclimate reconstructions from lake sediment oxygen isotope records and mass balance models." Geochimica et Cosmochimica Acta **105**: 342-359.

Steinman, B. A., et al. (2014). "Ocean‐ atmosphere forcing of centennial hydroclimate variability in the Pacific Northwest." Geophysical Research Letters **41**(7): 2553-2560.

Steinman, B. A., et al. (2019). "Lake sediment records of Holocene hydroclimate and impacts of the Mount Mazama eruption, north-central Washington, USA." Quaternary Science Reviews **204**: 17-36.

Steinman, B. A., et al. (2016). "Oxygen isotope records of Holocene climate variability in the Pacific Northwest." Quaternary Science Reviews **142**: 40-60.

Sun, W., et al. (2022). "Pacific multidecadal (50–70 year) variability instigated by volcanic forcing during the Little Ice Age (1250–1850)." Climate dynamics **59**(1-2): 231-244.

Svenning, J. C. and B. Sandel (2013). "Disequilibrium vegetation dynamics under future climate change." American Journal of Botany **100**(7): 1266-1286.

Torrence, C. and G. Compo (1998). A practical guide to wavelet analysis, B. Am. Meteorol. Soc., 79, 61–78.

Verbruggen, W., et al. (2021). "Contrasting responses of woody and herbaceous vegetation to altered rainfall characteristics in the Sahel." Biogeosciences **18**(1): 77-93.

Wagner, H. H. (2004). "Direct multi- scale ordination with canonical correspondence analysis." Ecology **85**(2): 342-351.

Walsh, M. K., et al. (2023). "Postglacial Fire and Vegetation History from Doheney Lake in the Sinlahekin Wildlife Area, Okanogan County, Washington." Northwest Science **96**(1-2): 1-21.

Walsh, M. K., et al. (2015). "A regional perspective on Holocene fire–climate–human interactions in the Pacific Northwest of North America." Annals of the Association of American Geographers **105**(6): 1135-1157.

Whitlock, C. and P. J. Bartlein (1997). "Vegetation and climate change in northwest America during the past 125 kyr." Nature **388**(6637): 57-61.

Whitlock, C., et al. (2012). "Holocene seasonal variability inferred from multiple proxy records from Crevice Lake, Yellowstone National Park, USA." Palaeogeography, Palaeoclimatology, Palaeoecology **331**: 90-103.

Whitlock, C. and C. Larsen (2001). "Charcoal as a fire proxy." Tracking environmental change using lake sediments: terrestrial, algal, and siliceous indicators: 75-97.

Williams, J. W., et al. (2021). "A unifying framework for studying and managing climate-driven rates of ecological change." Nature Ecology & Evolution **5**(1): 17-26.

Williams, J. W., et al. (2002). "Rapid and widespread vegetation responses to past climate change in the North Atlantic region." Geology **30**(11): 971-974.

Winkler, D. E., et al. (2019). "Shrub persistence and increased grass mortality in response to drought in dryland systems." Global change biology **25**(9): 3121-3135.

Wise, E. K. and M. P. Dannenberg (2017). "Reconstructed storm tracks reveal three centuries of changing moisture delivery to North America." Science advances **3**(6): e1602263.

Wright, H. E., et al. (1984). "Piston corers for peat and lake sediments." Ecology **65**(2): 657-659.

Declaration of interests

☒ The authors declare that they have no known competing financial interests or personal relationships that could have appeared to influence the work reported in this paper.

☐ The author is an Editorial Board Member/Editor-in-Chief/Associate Editor/Guest Editor for *[Journal name]* and was not involved in the editorial review or the decision to publish this article.

☐ The authors declare the following financial interests/personal relationships which may be considered as potential competing interests: